

Conformal Prediction Bands for Two-Dimensional Functional Time Series

Niccolò Ajroldi^a, Jacopo Diquigiovanni^b, Matteo Fontana^{c,*}, Simone Vantini^a

^a*MOX - Department of Mathematics, Politecnico di Milano, Milan (MI), Italy*

^b*Department of Statistical Sciences, University of Padova, Padova (PD), Italy*

^c*European Commission, Joint Research Centre (JRC), Ispra (VA), Italy*

Abstract

Conformal Prediction (CP) is a versatile nonparametric framework used to quantify uncertainty in prediction problems. In this work, we provide an extension of such method to the case of time series of functions defined on a bivariate domain, by proposing for the first time a distribution-free technique which can be applied to time-evolving surfaces. In order to obtain meaningful and efficient prediction regions, CP must be coupled with an accurate forecasting algorithm, for this reason, we extend the theory of autoregressive processes in Hilbert space in order to allow for functions with a bivariate domain. Given the novelty of the subject, we present estimation techniques for the Functional Autoregressive model (FAR). A simulation study is implemented, in order to investigate how different point predictors affect the resulting prediction bands. Finally, we explore benefits and limits of the proposed approach on a real dataset, collecting daily observations of Sea Level Anomalies of the Black Sea in the last twenty years.

Keywords: Conformal Prediction, Forecasting, Functional autoregressive process, Functional time series, Two-dimensional functional data, Uncertainty Quantification

*Email: matteo.fontana@ec.europa.eu

1. Introduction

Data observed on a two-dimensional domain arise naturally across several disciplines, motivating an increasing demand for dedicated analysis techniques. Functional Data Analysis (FDA) (Ramsay and Silverman 2005) is thus accruing interest as a valid option for representing such complex data, since it allows preserving their continuous nature, and provides a rigorous mathematical framework. Among the others, Zhou and Pan (2014) analyzed temperature tracking of specific areas, presenting and comparing two approaches for performing Functional Principal Component Analysis (FPCA) on functions defined on a non-rectangular domain, Porro-Muñoz et al. (2014) gave a detailed description of the entire imaging process using the FDA approach, proposing also a representation of iris images through functional data, while a novel regularization technique for Gaussian random fields on a rectangular domain has been proposed by Rakê (2010) and applied to 2D electrophoresis images. Another bivariate smoothing approach in a penalized regression framework is introduced by Ivanescu and Andrada (2013), allowing for the estimation of multiple functional parameters of completely or incompletely sampled two-dimensional functional data. As shown by Gervini (2010), also mortality rates can be interpreted as two-dimensional functional data, where one dimension is the temporal one and the other one refers to age.

Whereas in all the work reviewed above functions are assumed to be realization of *iid* or at least *exchangeable* random objects, to the best of our knowledge there is no literature focusing on forecasting of time-dependent two-dimensional functional data. In this work, we will focus on time series of surfaces, representing them as two-dimensional functional time series (FTS).

A two-dimensional functional time series is an ordered sequence Y_1, \dots, Y_T of random variables with values in a functional Hilbert space \mathbb{H} , characterized by some sort of temporal dependency. More formally, we consider a probability space $(\Omega, \mathcal{F}, \mathbb{P})$, and define a random function at time t as $Y_t : \Omega \rightarrow \mathbb{H}$, measurable with respect to the Borel σ -algebra $\mathcal{B}(\mathbb{H})$. In the rest of the article we will consider functions belonging to $\mathbb{H} = \mathcal{L}^2([c, d] \times [e, f])$, the space of measurable square integrable real-valued functions defined on the rectangle $[c, d] \times [e, f] \subset \mathbb{R}^2$, with $c, d, e, f \in \mathbb{R}$, $c < d$, $e < f$ ¹. We stress the fact that,

¹Such choice is motivated by many reasons, one above all is the fact that, by considering functions in $\mathcal{L}^2([c, d] \times [e, f])$, the usual Fréchet mean for functional data coincides with the pointwise mean and the covariance kernel coincides with the point-wise

from a theoretical point of view, our methodology can be applied to functions defined on a generic subset of \mathbb{R}^2 , however, for simplicity and without loss of generality, we will only consider rectangular domains.

Given a realization of such a stochastic process $\{Y_t\}_{t=1, \dots, N}$, we aim to forecast the next realization and, at the same time, quantify the uncertainty around the predicted function. Whereas uncertainty quantification in the context of *univariate* FTS forecasting has received increasing attention in the statistical community in recent decades, no attempts have been made to extend them to functions defined on a bidimensional domain. Specifically, most of the research has focused on adapting of the Bootstrap to the functional setting (see e.g. [Hyndman and Shang 2009](#) and [Rossini and Canale 2018](#)). However, the aforementioned Bootstrap procedure is very computationally intensive, especially in the infinite-dimensional context of functional data.

In this work, we will instead focus on Conformal Prediction (CP), another more recent and versatile nonparametric approach to prediction. The first appearance of such technique dates back in [Gammerman et al. \(1998\)](#) and it has been later presented in great details in the book of [Vovk et al. \(2005\)](#) and in [Balasubramanian et al. \(2006\)](#). A recent review of the theory of Conformal inference can be found in [Fontana et al. \(2022\)](#). In a nutshell, the CP approach is based on the idea of assigning scores to new candidate realizations in order to assess their non-conformity with respect to other observed data. Prediction sets are then derived by inverting the hypothesis test obtained using such scores, including only candidate realizations with a conformity level higher than a suited and properly selected threshold. The attractiveness of Conformal Prediction relies on its great generality and versatility, which permits to couple it with potentially any predictive algorithm, in order to obtain distribution free prediction sets.

We will consider only the Inductive Conformal Prediction a.k.a. Split Conformal Prediction method ([Papadopoulos et al. 2002](#)). Such modification of the original Transductive Conformal method is not only computationally efficient, but is also necessary in high-dimensional frameworks like the one of functional data. Indeed, the main drawback of the Full Conformal approach is that the prediction algorithm needs to be trained again for every possi-

covariance. Moreover, \mathbb{H} is a separable Hilbert space, with the usual inner product: $\langle x, y \rangle := \int_c^d \int_e^f x(u, v) y(u, v) du dv \quad \forall x, y \in \mathbb{H}$

ble candidate realization y . In practice, in multivariate problems, where y lies in \mathbb{R}^p , one runs the above routine for candidate y over a p -dimensional grid. While such approach is prohibitive for high-dimensional spaces, since computational times grow exponentially with p , it is actually unfeasible in a functional setting, in which y lies in an infinite-dimensional space. On the contrary, employing Split Conformal inference along with a specific family of nonconformity scores, introduced by [Diquigiovanni et al. \(2021b\)](#) and explicitly tailored to functional data, permits deriving prediction sets in closed form.

It is important to notice that the theory of CP is developed under the only assumption of exchangeable data. Such very mild hypothesis, despite being one of the strengths of CP, is clearly not suitable for the time series context, in which one has to deal with temporal dependence between data. Adapting CP beyond exchangeable data has recently gathered attention in the statistical community. [Chernozhukov et al. \(2018\)](#) rephrased the CP framework in the context of randomization inference, proving approximate validity of the resulting prediction sets under weak assumptions on the conformity scores and on the ergodicity of the time series. Later, [Diquigiovanni et al. \(2021a\)](#) adapted such methodology to allow for functional time series in a Split Conformal setting. We will extend such method to two-dimensional functional data. At the same time, we will propose different point predictors for 2D FTS, eventually comparing them in an order to assess how forecasting performances influence the amplitude of the resulting prediction band.

The rest of this paper is as follows: we start by introducing Conformal Prediction methodology for two-dimensional functional data in [Section 2](#), providing theoretical guarantees on the resulting prediction bands. In [Section 3](#), we introduce different point-prediction algorithms for two-dimensional functional time series, proposing for the first time an extension of the Functional Autoregressive Model for two-dimensional functional data. Such forecasting algorithms are then adapted to the Conformal inference setting and consequently compared by means of the resulting prediction bands in a simulation study in [Section 4](#). Finally, in [Section 5](#) we employ the developed techniques to obtain forecasts and prediction bands in a real scenario, predicting day by day the sea level over the Black Sea. [Section 6](#) concludes.

2. Methodology: Conformal Prediction for 2D Functional Data

Consider a time series Z_1, \dots, Z_T of regression pairs $Z_t = (X_t, Y_t)$, with $t = 1, \dots, T$. Let Y_t be a random variable with values in \mathbb{H} , while X_t is a set of random covariates at time t belonging to a measurable space. Notice that X_t is a generic set of regressors, which may contain both exogenous and endogenous variables. In particular, later in the manuscript, we will consider X_t to contain only the lagged version of the function Y_t , namely Y_{t-1} . Given a significance level $\alpha \in [0, 1]$, we aim to design a procedure that outputs a prediction set $\mathcal{C}_{T,1-\alpha}(X_{T+1})$ for Y_{T+1} based on Z_1, \dots, Z_T and X_{T+1} , with unconditional coverage probability close to $1 - \alpha$. More formally, we define $\mathcal{C}_{T,1-\alpha}(X_{T+1})$ to be a *valid* prediction set if:

$$\mathbb{P}(Y_{T+1} \in \mathcal{C}_{T,1-\alpha}(X_{T+1})) \geq 1 - \alpha \quad (1)$$

Specifically, we would like to construct a particular type of prediction sets, commonly known as *prediction bands*, formally defined as:

$$\{y \in \mathbb{H} : y(u, v) \in B_n(u, v) \quad \forall (u, v) \in [c, d] \times [e, f]\} \quad (2)$$

where $B_n(u, v) \subseteq \mathbb{R}$ is an interval for each $(u, v) \in [c, d] \times [e, f]$. The convenience of such type of prediction sets in applications is extensively motivated in the literature (see e.g. [López-Pintado and Romo 2009](#), [Lei et al. 2015](#) and [Diquigiovanni et al. 2021b](#)), since a prediction set of this type can be visualized easily, a property that is instead not guaranteed if the prediction region is a generic subset of \mathbb{H} .

Let z_1, \dots, z_T be realizations of Z_1, \dots, Z_T . As the name suggests, Split Conformal inference is based on a random split of data into two disjoint sets: let $\mathcal{I}_1, \mathcal{I}_2$ be a random partition of $\{1, \dots, T\}$, such that $|\mathcal{I}_1| = m$, $|\mathcal{I}_2| = l$, $m, l \in \mathbb{N}$ $m, l > 0$, $m + l = T$. Historical observations z_1, \dots, z_T are divided into a *training set* $\{z_h, h \in \mathcal{I}_1\}$, from which we will estimate the model, and a *calibration set* $\{z_h, h \in \mathcal{I}_2\}$, that will be used in an out-of-sample context to measure the nonconformity of a new candidate function. The choice of the split ratio and of the type of split is non-trivial and has motivated discussion in the statistical community. We will fix the training-calibration ratio equal to 1 and perform a random split, but we refer to [Appendix A](#) for a more extensive discussion on these issues.

We then introduce a *nonconformity measure* \mathcal{A} , which is a measurable function with values in $\mathbb{R} \cup \{+\infty\}$. The role of $\mathcal{A}(\{z_h, h \in \mathcal{I}_1\}, z)$ is to

quantify the nonconformity of a new datum z with respect to the training set $\{z_h, h \in \mathcal{I}_1\}$. The choice of the nonconformity measure is crucial if we aim to find prediction bands (2) and if we want to find them in closed form. Moreover, as will be discussed later, this choice will also affect the size of the resulting prediction bands, and thus their efficiency. Motivated by such considerations, we will employ the following nonconformity score, introduced by [Diquigiovanni et al. \(2021b\)](#), extended here to two-dimensional functional data:

$$\mathcal{A}(\{z_h : h \in \mathcal{I}_1\}, z) = \operatorname{ess\,sup}_{(u,v) \in [c,d] \times [e,f]} \frac{|y(u,v) - g_{\mathcal{I}_1}(u,v; x_{T+1})|}{s_{\mathcal{I}_1}(u,v)} \quad (3)$$

where $z = (x_{T+1}, y)$, $g_{\mathcal{I}_1}$ is a point predictor built from the training set \mathcal{I}_1 , and $s_{\mathcal{I}_1}$ is a *modulation function*, which is a positive function depending on \mathcal{I}_1 itself that allows for prediction bands with non-constant width along the domain. The estimation of $g_{\mathcal{I}_1}$ is discussed in Section 4, while the functional standard deviation will be employed as modulation function $s_{\mathcal{I}_1}$, allowing for wider bands in the parts of the domain where data show high variability and narrower and more informative prediction bands in those parts characterized by low variability. For an extensive discussion on the optimal choice of modulation function, we refer to [Diquigiovanni et al. \(2021b\)](#).

Consider now a candidate function $y \in \mathbb{H}$ and define the augmented dataset as $Z_{(y)} = \{Z_t\}_{t=1}^{T+1}$, where:

$$Z_t = \begin{cases} (X_t, Y_t), & \text{if } 1 \leq t \leq T \\ (X_{T+1}, y), & \text{if } t = T + 1 \end{cases} \quad (4)$$

The key idea of the methodology proposed by [Chernozhukov et al. \(2018\)](#) and extended by [Diquigiovanni et al. \(2021a\)](#) is to generate several randomized versions of $Z_{(y)}$ through a specifically tailored permutation scheme, and compute nonconformity scores on each of them. We will then decide whether to include y in the prediction region, by comparing the nonconformity score of $Z_{(y)}$ with that of its permuted replicas.

In order to do so, we aim to define a family Π of index permutations $\pi : \{1, \dots, T+1\} \rightarrow \{1, \dots, T+1\}$, that leaves unchanged the indices of the training set, and modify only $\{\mathcal{I}_2, T+1\}$, namely the indices of the calibration set and the next time step. In order to do so, let's first introduce a function $\lambda : \{\mathcal{I}_2, T+1\} \rightarrow \{1, \dots, l+1\}$ such that $\lambda(t)$ returns the t -th element of the ordered set $\{\mathcal{I}_2, T+1\}$. Fix now a positive integer $b \in$

	T						T+1
t	1	2	3	4	5	6	7
$\lambda(t)$	/	1	/	2	3	/	4
$\tilde{\pi}_1(\lambda(t))$	/	1	/	2	3	/	4
$\tilde{\pi}_2(\lambda(t))$	/	3	/	4	1	/	2
$\pi_1(t)$	1	2	3	4	5	6	7
$\pi_2(t)$	1	5	3	7	2	6	4

Training set

Calibration set

Test set

Figure 1: Example of permutation families $\tilde{\Pi}$ and Π , with sample size $T = 6$, training set $\mathcal{I}_1 = \{1, 3, 6\}$, calibration set $\mathcal{I}_2 = \{2, 4, 5\}$, $l = m = 3$, size of blocking scheme $b = 2$. In this case $\lambda : \{\mathcal{I}_2, T + 1\} \equiv \{2, 4, 5, 7\} \rightarrow \{1, 2, 3, 4\}$, $\tilde{\Pi} = \{\tilde{\pi}_1, \tilde{\pi}_2\}$ and $\Pi = \{\pi_1, \pi_2\}$.

$\{1, \dots, l + 1\}$ such that $\frac{l+1}{b} \in \mathbb{N}$ and define a family $\tilde{\Pi}$ of index permutations that acts on the set $\{1, \dots, l + 1\}$. Each $\tilde{\pi}_i \in \tilde{\Pi}$ is required to be a bijection $\tilde{\pi}_i : \{1, \dots, l + 1\} \rightarrow \{1, \dots, l + 1\}$, for $i = 1, \dots, \frac{l+1}{b}$. In particular, we will consider non-overlapping blocking permutations, with b representing the size of the blocking scheme:

$$\tilde{\pi}_i(j) = \begin{cases} j + (i - 1)b & \text{if } 1 \leq j \leq l - (i - 1)b + 1 \\ j + (i - 1)b - l - 1 & \text{if } l - (i - 1)b + 2 \leq j \leq l + 1 \end{cases} \quad (5)$$

By definition, we have that $|\tilde{\Pi}| = \frac{l+1}{b}$. Moreover, such family of transformations forms an algebraic group, containing among other the identity transformation $\tilde{\pi}_1$. It is then straightforward to introduce the family Π of index permutations acting on $\{1, \dots, T + 1\}$. Each $\pi_i \in \Pi$, with $i = 1, \dots, \frac{l+1}{b}$ is defined as:

$$\pi_i(t) = \begin{cases} t & \text{if } t \in \mathcal{I}_1 \\ \lambda^{-1}(\tilde{\pi}_i(\lambda(t))) & \text{if } t \in \mathcal{I}_2 \cup \{T + 1\} \end{cases} \quad (6)$$

In Figure 1 is reported a trivial example of the families of permutation Π and $\tilde{\Pi}$.

We refer to $Z_{(y)}^\pi = \{Z_{\pi(t)}\}_{t=1}^{T+1}$ as the randomized version of $Z_{(y)} = \{Z_t\}_{t=1}^{T+1}$. Let's then define the randomization p-value as:

$$p(y) = \frac{1}{|\Pi|} \sum_{\pi \in \Pi} \mathbf{1}(S(Z_{(y)}^\pi) \geq S(Z_{(y)})) \quad (7)$$

where the nonconformity scores $S(Z_{(y)})$ and $S(Z_{(y)}^\pi)$ are defined as:

$$S(Z_{(y)}) = \mathcal{A}(\{Z_h : h \in \mathcal{I}_1\}, Z_{T+1}) \quad (8)$$

$$S(Z_{(y)}^\pi) = \mathcal{A}(\{Z_h : h \in \mathcal{I}_1\}, Z_{\pi(T+1)}) \quad (9)$$

The idea is to apply permutations, modifying the order of observations in the calibration set, while at the same time preserving the dependence between them, thanks to the block structure of Π . For each π , we compute the nonconformity score of $Z_{(y)}^\pi$. The p-value of a test candidate value y is then determined as the proportion of randomized versions $Z_{(y)}^\pi$ with a higher or equal nonconformity score than the one of the original augmented dataset $Z_{(y)}$. Notice that $p(y)$ is a measure of the *conformity* of the candidate function y with respect to the permutation family Π . It is then natural to include in the prediction set only functions y with an “high” conformity level. Therefore, in accordance with Conformal Prediction, given a significance level $\alpha \in [b/(l+1), 1]^2$, we define the prediction bands by test inversion:

$$\mathcal{C}_{T,1-\alpha}(X_{T+1}) := \{y \in \mathbb{H} : p(y) > \alpha\} \quad (10)$$

As mentioned before, the advantage of using the Split Conformal method along with the conformity measure (3) relies on the possibility to find the prediction set in closed form. By defining k^s as the $\lceil (|\Pi| + 1)(1 - \alpha) \rceil$ th smallest value of $\{S(Z_{(y)}^\pi), \pi \in \Pi \setminus \pi_1\}$, we can derive a prediction band in closed form:

$$\begin{aligned} y \in \mathcal{C}_{T,1-\alpha}(X_{T+1}) &\iff p(y) > \alpha \\ &\iff S(Z_{(y)}) \leq k^s \\ &\iff \operatorname{ess\,sup}_{(u,v) \in [c,d] \times [e,f]} \frac{|y(u,v) - g_{\mathcal{I}_1}(u,v; x_{T+1})|}{s_{\mathcal{I}_1}(u,v)} \leq k^s \\ &\iff |y(u,v) - g_{\mathcal{I}_1}(u,v; x_{T+1})| \leq k^s s_{\mathcal{I}_1}(u,v) \quad \forall (u,v) \in [c,d] \times [e,f] \\ &\iff y(u,v) \in [g_{\mathcal{I}_1}(u,v; x_{T+1}) \pm k^s s_{\mathcal{I}_1}(u,v)] \quad \forall (u,v) \in [c,d] \times [e,f] \end{aligned}$$

The prediction band is therefore:

$$\mathcal{C}_{T,1-\alpha}(X_{T+1}) := \{y \in \mathbb{H} : y(u,v) \in [g_{\mathcal{I}_1}(u,v; x_{T+1}) \pm k^s s_{\mathcal{I}_1}(u,v)] \forall (u,v) \in [c,d] \times [e,f]\} \quad (11)$$

²If $\alpha \in (0, b/(l+1))$ the resulting prediction set will coincide with the entire space \mathbb{H} .

In the case in which regression pairs are exchangeable, the proposed method retains exact, model-free validity (Chernozhukov et al. 2018). However, when such assumption is not met, one can guarantee only approximately validity (in the sense of Theorem 1) of the proposed approach under weak assumptions on the conformity score and the ergodicity of the time series.

More formally, let \mathcal{A}^* be an oracle nonconformity measure, inducing oracle nonconformity score S^* . Define F to be the cumulative (unconditional) distribution function of the oracle nonconformity scores, namely $F(x) = \mathbb{P}(S^*(Z_{(y)}^\pi) < x)$ and \hat{F} the empirical counterpart, obtained by applying permutations $\pi \in \Pi$: $\hat{F}(x) := \frac{1}{|\Pi|} \sum_{\pi \in \Pi} \mathbb{1}\{S^*(Z_{(y)}^\pi) < x\}$. Let $\{\delta_{1\bar{l}}, \delta_{2\bar{m}}, \gamma_{1\bar{l}}, \gamma_{2\bar{m}}\}$ be sequences of numbers converging to zero. Moving from Chernozhukov et al. (2018), Theorem 1 of Diquigiovanni et al. (2021a) prescribes sufficient conditions in order to guarantee asymptotic exactness of the prediction set. We report such result with a slightly modified notation. Let here $Z = Z_{(Y_{T+1})}$, where the candidate function y is now substituted by the random function Y_{T+1} .

Theorem 1. *If the following conditions hold:*

- $\sup_{a \in \mathbb{R}} |\hat{F}(a) - F(a)| \leq \delta_{1\bar{l}}$ with probability $1 - \gamma_{1\bar{l}}$
- $\frac{1}{|\Pi|} \sum_{\pi \in \Pi} \left[S(Z^\pi) - S^*(Z_{(y)}^\pi) \right]^2 \leq \delta_{2\bar{m}}^2$ with probability $1 - \gamma_{2\bar{m}}$
- $|S(Z^\pi) - S^*(Z^\pi)| \leq \delta_{2\bar{m}}$ with probability $1 - \gamma_{2\bar{m}}$
- With probability $1 - \gamma_{2\bar{m}}$ the pdf of $S^*(Z^\pi)$ is bounded above by a constant D

then the Conformal confidence set has approximate coverage α :

$$|\mathbb{P}(Y_{T+1} \in \mathcal{C}_{T,1-\alpha}(X_{T+1}) - (1-\alpha))| \leq 6\delta_{1\bar{l}} + 2\delta_{2\bar{m}} + 2D \left(\delta_{2\bar{m}} + 2\sqrt{\delta_{2\bar{m}}} \right) + \gamma_{1\bar{l}} + \gamma_{2\bar{m}} \quad (12)$$

The first condition concerns the approximate ergodicity of \hat{F} for F , a condition which holds for strongly mixing time series using blocking permutation Π defined in (6) (Chernozhukov et al. 2018). The other conditions are requirements for the quality of approximating the oracle $S^*(Z^\pi)$ with $S(Z^\pi)$. Intuitively, $\delta_{2\bar{m}}^2$ bounds the discrepancy between the nonconformity scores and their oracle counterparts. Such condition is related to the quality of the point prediction and to the choice of the employed nonconformity measure.

3. Point prediction

In order to obtain CP band with empirical coverage close to the nominal one while maintaining a small width, the choice of an accurate point predictor is crucial. As mentioned before, whereas in the typical i.i.d. case finite-sample unconditional coverage still holds when the model is heavily misspecified (Diquigiovanni et al. 2021b), in the time series context a strong model misspecification may compromise the coverage guarantees and not only the efficiency of the resulting prediction bands (Chernozhukov et al. 2018, Diquigiovanni et al. (2021a)).

For this reason, it is important to consider models that are consistent with the functional nature of the observations and that can adequately deal with their infinite dimensionality. We hence extend for the first time the theory of autoregressive processes in Hilbert space, in order to allow for temporarily evolving surfaces, i.e. for time series of functions with a bivariate domain. Given the novelty of the subject, we introduce the Functional Autoregressive model (FAR) in Section 3.1 and propose estimation techniques for it in Section 3.2.

3.1. FAR(1) Model

One of the most popular statistical models used to capture temporal dependence between functional observations is the functional autoregressive process (FAR). The theory of functional autoregressive processes in Hilbert spaces is developed in the pioneering monograph of Bosq (2000) and a comprehensive collection of statistical advancements for the FAR model can be found in the book by Horváth and Kokoszka (2012). A sequence of mean zero random functions $\{Y_t\}_{t=1}^T \subset \mathbb{H}$ follows a non-concurrent functional autoregressive process of order 1 if:

$$Y_t = \Psi Y_{t-1} + \varepsilon_t \quad t = 2, \dots, T \quad (13)$$

where $\{\varepsilon_t\}_{t \in \mathbb{N}}$ is a sequence of iid mean-zero innovation errors with values in \mathbb{H} satisfying $\mathbb{E}[||\varepsilon_t||^2] < +\infty$ and Ψ is a linear bounded operator from \mathbb{H} to itself. In particular, we will consider Ψ to be a Hilbert-Schmidt operator with kernel ψ , in such a way that:

$$(\Psi x)(u, v) = \int_c^d \int_e^f \psi(u, v; w, z) x(w, z) dw dz \quad \forall x \in \mathbb{H}, \forall (u, v) \in [c, d] \times [e, f] \quad (14)$$

In order to ensure existence of a stationary solution to the FAR(1) equation (13), one has to require the existence of an integer $j_0 \in \mathbb{N}$ such that $\|\Psi\|^{j_0} < 1$ (Bosq 2000, Lemma 3.1).

3.2. FAR(1) Estimation

We first introduce a model that may appear simplistic, since it does not exploit the possible time dependence between the values of the function in different points of the functional domain, but that in practical applications provides satisfying results. The prediction method assumes an autoregressive structure in each location (u, v) of the domain, ignoring the dependencies between different points. More formally, we define the *concurrent* FAR(1) as:

$$Y_t(u, v) = \psi_{u,v} Y_{t-1}(u, v) + \varepsilon_t(u, v) \quad \forall (u, v) \in [c, d] \times [e, f] \quad (15)$$

where $\psi_{u,v} \in \mathbb{R}$ and $t = 2, \dots, T$. Supposing to have observed functional data y_1, \dots, y_T on a common two-dimensional grid $\{(u_i, v_j)\}$ with $i = 1, \dots, N_1$ and $j = 1, \dots, N_2$, the goal becomes to estimate ψ_{u_i, v_j} for each location (u_i, v_j) in the grid. We will later refer to this model as **FAR(1)-Concurrent**.

Following a procedure similar to the Yule-Walker estimation in the scalar setting, we propose now a more sophisticated estimator of Ψ . Proceeding similarly to Horváth and Kokoszka (2012), we derive the following estimator:

$$\hat{\Psi}_{Mx} = \frac{1}{T-1} \sum_{i,j=1}^M \sum_{t=1}^T \hat{\lambda}_j \langle x, \hat{\xi}_j \rangle \langle Y_{t-1}, \hat{\xi}_j \rangle \langle Y_t, \hat{\xi}_i \rangle \hat{\xi}_i \quad \forall x \in \mathbb{H} \quad (16)$$

where ξ_1, \dots, ξ_M are the first M normalized functional principal components (FPC's), $\lambda_1, \dots, \lambda_M$ are the corresponding eigenvalues and $\langle x, \xi_1 \rangle, \dots, \langle x, \xi_M \rangle$ are the scores of x along the FPC's. Appendix C is dedicated to the illustration of two different estimation techniques for ξ_i and λ_i , one based on a discretization of functions on a fine grid and the other designed starting from an expansion of data on a finite basis system. We further refer to Appendix B for more details on the derivation of estimator (16) and for an extensive discussion on how to adapt it to the Conformal Prediction setting, in order to estimate Ψ from the training set \mathcal{I}_1 only.

A different yet simpler forecasting procedure has been proposed by Aue et al. (2012) for one dimensional functional data and will be here extended to the two-dimensional setting. Calling once again ξ_1, \dots, ξ_M the first M functional principal components, we decompose the functional time series as

follows:

$$Y_t(u, v) = \sum_{j=1}^M \langle Y_t, \xi_j \rangle \xi_j(u, v) + e_t(u, v) = \quad (17)$$

$$= \mathbf{Y}_t^T \boldsymbol{\xi}(u, v) + e_t(u, v) \quad (18)$$

where $\mathbf{Y}_t = [\langle Y_t, \xi_1 \rangle, \dots, \langle Y_t, \xi_M \rangle]^T$ contains the scores of the projection, $\boldsymbol{\xi}(u, v) = [\xi_1(u, v), \dots, \xi_M(u, v)]^T$ and $e_t(u, v)$ is the approximation error due to the truncation of the expansion on the first M principal components. Neglecting the approximation error e_t , one can prove that the vector \mathbf{Y}_t follows a multivariate autoregressive process of order 1. Plugging in the estimated FPCs $\hat{\xi}_1, \dots, \hat{\xi}_M$, we can estimate the parameters of the resulting model using standard techniques of multivariate statistics and forecast $\hat{\mathbf{Y}}_{T+1}$ based on historical data Y_1, \dots, Y_T . The predicted function \hat{Y}_{T+1} can be simply reconstructed as:

$$\hat{Y}_{T+1}(u, v) = \hat{\mathbf{Y}}_{T+1}^T \boldsymbol{\xi}(u, v) \quad (19)$$

Throughout the rest of the work, we will employ all the estimators presented above, comparing them in Section 4 in terms of prediction performances.

4. Simulation study

4.1. Study Design

In this section, we will evaluate the procedure presented above through a simulation study. The goal is twofold: we aim to assess the quality of the proposed Conformal Prediction bands and, at the same time, evaluate different point predictors in terms of the resulting prediction regions. We will employ as a data generating process a FAR(1) model in order to compare the different estimation routines presented in Section 3.1. In order to fix a benchmark on the forecasting performances, we will employ as reference prediction algorithm the following naive one: $\hat{Y}_{T+1} = Y_T$. Notice that, by including a forecasting algorithm that is not coherent with the data generating process, we can illustrate how the presented CP procedure performs when a good point predictor $g_{\mathcal{I}_1}$ is not available. Although as reported in Section 3 an accurate forecasting algorithm is necessary to guarantee asymptotic validity, we will see that in the performed simulations CP bands will be valid even when such assumption does not hold.

Since this work is focused on uncertainty quantification of prediction in the context of two-dimensional functional data, we will compare forecasting performances by means of the resulting Conformal Prediction bands. Firstly and foremost, we will estimate the unconditional coverage by computing the *empirical unconditional coverage* in order to compare it with the nominal confidence level $1 - \alpha$. In the second place, we will consider the size of the prediction bands obtained since, intuitively, a small prediction band is preferable because it includes subregions of the sample space where the probability mass is highly concentrated (Lei et al. 2015) and it is typically more informative in practical applications.

In each scenario, we will compare the performances of five selected prediction algorithms, one of which do not exploit the autoregressive structure. To obtain further insights, we also include the errors obtained by assuming perfect knowledge of the operator Ψ . For ease of reference, we briefly describe these methods, and introduce some convenient notation.

- **FAR(1)-Concurrent** refers to the forecasting algorithm based on the estimation of the concurrent FAR(1) model (15).
- **FAR(1)-EK** (Estimated Kernel) denotes the first estimation procedure presented in Section 3.1, where we explicitly compute $\hat{\Psi}_M$ as prescribed by (16) and then set $\hat{Y}_{T+1} = \hat{\Psi}_M Y_T$.
- **FAR(1)-EK+** (Estimated Kernel improved) is a modification of the above method, where eigenvalues $\hat{\lambda}_i$ are replaced by $\hat{\lambda}_i + 1.5(\hat{\lambda}_1 + \hat{\lambda}_2)$, as recommended by Didericksen et al. (2010) and further discussed in Appendix B.
- **FAR(1)-VAR** denotes the forecasting procedure (19), where we exploit the expansion on estimated functional principal components and forecast Y_{T+1} using the underlying VAR(1) model.
- **Naive**: we just set $\hat{Y}_{T+1} = Y_T$. This method does not attempt to model temporal evolution, it is included to see how much can be gained by exploiting the autoregressive structure of data.
- **Oracle**: we set $Y_{T+1} = \Psi Y_T$, using the actual Ψ from which data are simulated. This point predictor is clearly not available in practical application, but it is interesting to include it in order to see if poor predictions might be due to poor estimation of Ψ .

When it is required (namely in FAR(1)-EK, FAR(1)-EK+, FAR(1)-VAR), FPCA is performed using the discretization approach, as motivated in [Appendix C](#). The number of principal components is selected by the cumulative proportion of variance criterion. Calling $\hat{\lambda}_1, \dots, \hat{\lambda}_M$ the M largest estimated eigenvalues, we choose $M \in \mathbb{N}$ such that $\sum_{j=1}^M \hat{\lambda}_j / \sum_{j=1}^{\infty} \hat{\lambda}_j$ exceeds a pre-determined percentage value, in this case fixed equal to 0.8. We noticed that, on average, this entails to select a number of harmonics equal to 5.

Throughout the whole simulation study, we set the significance level $\alpha = 0.1$. In the first simulation, in [Section 4.2](#), we will fix the size b of the blocking scheme (6) equal to 1 and the sample size T will take values 19, 49, 99, 499. Secondly, in [Section 4.3](#), we will instead keep the sample size fixed equal to 119 and repeat the simulations with $b = 1, 3, 6$. As usually done in the time series setting, the first observation is taken into account as a covariate only and will neither take part of the training set, nor of the calibration set. The proportion of data in the training and in the calibration set are hence equal to one half of the remaining observations: $m = l = (T - 1)/2$. For each value of T , we repeat the procedure by considering $N = 1000$ simulations. The simulations are performed using the R Programming Language ([R Core Team 2020](#)).

Extending the implementation of [Hörmann and Łukasz \(2017\)](#), in order to simulate a sequence of functions $\{Y_t\}_{t=1, \dots, T}$ from a functional autoregressive process of order one, we assume that observations lie in a finite dimensional subspace of the function space \mathbb{H}^3 , spanned by orthonormal basis functions ϕ_1, \dots, ϕ_M , with $M \in \mathbb{N}$ representing the dimension of such subspace. Therefore, we have:

$$Y_t(u, v) = \phi(u, v)^T \mathbf{Y}_t \quad (20)$$

$$\varepsilon_t(u, v) = \phi(u, v)^T \boldsymbol{\varepsilon}_t \quad (21)$$

$$\psi(u, v; w, z) = \phi(u, v)^T \boldsymbol{\Psi} \mathbf{W} \phi(w, z) \quad (22)$$

where $\phi(u, v) = [\phi_1(u, v), \dots, \phi_M(u, v)]^T \in \mathbb{R}^M$, $\forall (u, v) \in [0, 1] \times [0, 1]$, $\mathbf{Y}_t, \boldsymbol{\varepsilon}_t \in \mathbb{R}^M$, $\forall t = 1, \dots, T$ and $\boldsymbol{\Psi} \in \mathbb{R}^{M \times M}$ and $\mathbf{W} \in \mathbb{R}^{K \times K}$, defined as $\mathbf{W} := \int_c^d \int_e^f \phi(u, v) \phi(u, v)^T du dv$. It follows that:

$$\mathbf{Y}_t = \boldsymbol{\Psi} \mathbf{Y}_{t-1} \mathbf{W} + \boldsymbol{\varepsilon}_t \quad t = 1, \dots, T \quad (23)$$

³Without loss of generality, throughout this section we will consider functions in $\mathbb{H} = \mathcal{L}^2([0, 1] \times [0, 1])$.

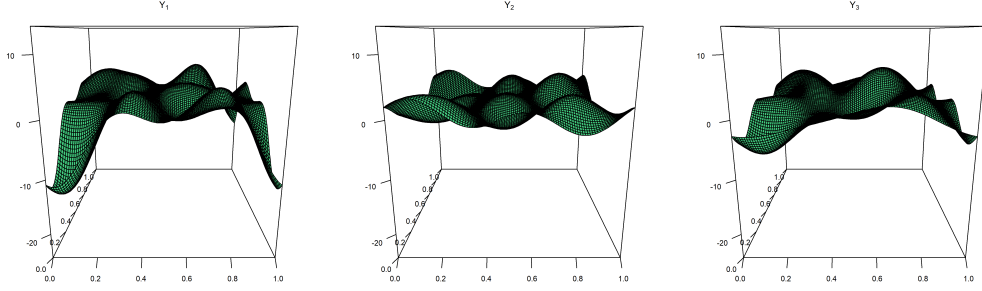


Figure 2: Example of the first three realizations (Y_1, Y_2, Y_3) of a simulated Functional Autoregressive Process of order one.

The basis system ϕ_1, \dots, ϕ_M is constructed as the tensor product basis of two cubic B-spline systems $\{g_i\}_{i=1, \dots, M_1}$, $\{h_j\}_{j=1, \dots, M_2}$, both defined on $[0, 1]$. We set $M_1 = M_2 = 5$, in such a way that $M = 25$. Notice that, by including more functions, we will better approximate the space \mathbb{H} , though inevitably producing rougher curves. On the other hand, by reducing the size of the basis system, one renounce to have a good representation of \mathbb{H} , but this permits to obtain smoother functions. The choice proposed for M is arbitrary, but provides a good compromise between the two outlined extremes. For an exhaustive discussion on the tensor product basis system, we refer to [Appendix C.2](#) The matrix Ψ is defined as $\Psi := 0.9 \frac{\tilde{\Psi}}{\|\tilde{\Psi}\|_F}$, with $\tilde{\Psi}$ having diagonal values equal to 0.8 and out-diagonal elements equal to 0.3⁴ Innovation errors ε_t are independently sampled from a multivariate Student's t -distribution, with 4 degrees of freedom and scale matrix having diagonal elements equal to 0.5 and out-diagonal entries equal to 0.3.

We report in [Figure 2](#) an example of the first three realizations of a simulated Functional Autoregressive Process of order one, represented on a grid of 10^4 points⁵.

⁴One can easily prove that, if relation (22) holds, then $\|\Psi\| = \|\Psi\|_F$, where $\|\cdot\|$ is the usual operatorial norm and $\|\cdot\|_F$ denotes the Frobenius norm.

⁵A GIF of the FAR(1) process evolution can be found at [GitHub repository](#) “Functional-Autoregressive-Process-2D”.

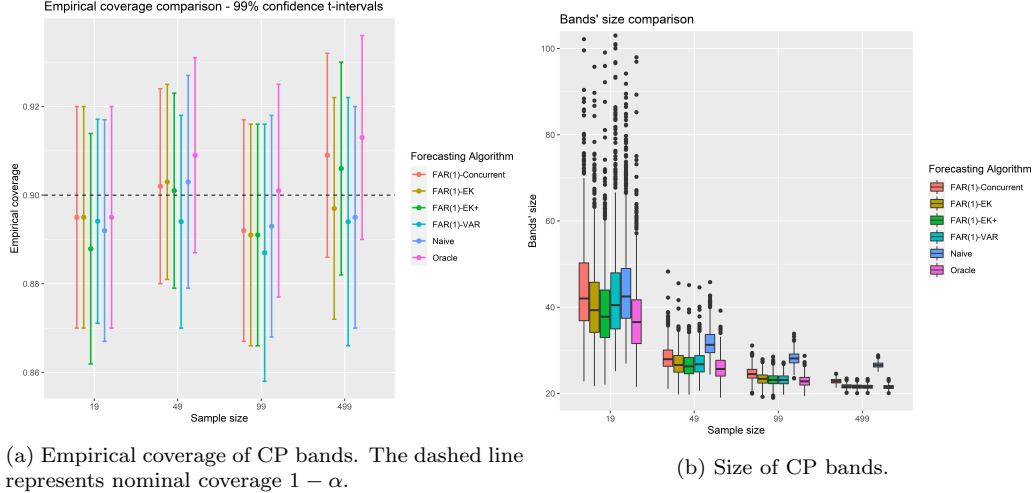


Figure 3: Results of first simulation study.

4.2. Increasing the Sample Size

As mentioned before, we first fix the size b of the blocking scheme equal to 1 and let the sample size T take values 19, 49, 99, 499.

Figure 3a shows the empirical coverage, together with the related 99% confidence interval. Specifically, the empirical coverage is computed as the fraction of the $N = 1000$ replications in which y_{T+1} belongs to $\mathcal{C}_{T,1-\alpha}(x_{T+1})$, and the confidence interval is reported in order to provide insights into the variability of the phenomenon in various scenarios, rather than to draw inferential conclusions about the unconditional coverage. Notice that different point predictors will intrinsically have dissimilar coverages, consequently this analysis aims to compare forecasting algorithm in terms of their predictive performances. We can appreciate that, in all the cases, the 99% confidence interval for the empirical coverage includes the nominal confidence level, regardless of the sample size at disposal. Moreover, it's interesting to notice that, even when an accurate forecasting algorithm $g_{\mathcal{I}_1}$ is not available (namely with FAR(1)-Concurrent and Naive), the proposed CP procedure still outputs prediction regions with an appropriate unconditional coverage.

Similarly to Diquigiovanni et al. (2021b), we define the size of a two-dimensional prediction band as the *volume* between the upper and the lower surfaces that define the prediction band:

$$\mathcal{Q}(s_{\mathcal{I}_1}) := \int_0^1 \int_0^1 2k s_{\mathcal{I}_1}(u, v) du dv = 2k \quad (24)$$

Measuring the size of the correspondent prediction bands, we can compare the efficiency of different forecasting routines. We stress the fact that distinct point predictors may guarantee potentially different coverages. For this reason, it is crucial to first evaluate the empirical coverage of the resulting prediction bands and only afterwards investigate their size.

Figure 3b reports the boxplots concerning the size of the $N = 1000$ prediction bands. One can notice that the size tends to decrease as long as the number of observations T increases, hence improving the efficiency of the prediction sets. As expected, Naive predictor provides larger prediction bands and while the difference is milder with small sample sizes, when T grows the size of the prediction regions of other methods systematically dominates the Naive's one. On the other hand, FAR(1)-EK and FAR(1)-EK+, that are both based on the estimation of autoregressive operator Ψ , provide the tightest prediction bands, not only when numerous observations are available, but also in small sample sizes scenario. Moreover, one can notice that FAR(1)-EK+ do not significantly improves FAR(1)-EK neither in terms of coverage, nor in terms of band size. We acknowledge that, when $T = 19$, VAR-efpc performs remarkably worse than the other methods. Indeed, the aforementioned method produces wider prediction bands, which are further source of the higher empirical coverage in Figure 3a. However, when the sample size increases, such forecasting algorithm performs comparably with the already mentioned FAR(1)-EK and FAR(1)-EK+. Finally, although the Conformal Prediction bands produced by the oracle predictor are obviously the most performing one, we can appreciate that both FAR(1)-EK and FAR(1)-EK+ provide CP bands with coverage and size comparable to the theoretically perfect oracle forecasting method.

4.3. Increasing the Blocking Scheme Size

We repeat here the previous simulation with fixed sample size T and a blocking scheme of increasing size b , in order to determine how the validity and efficiency of the resulting prediction bands are influenced by such parameter b . The value of T is fixed equal to 99, which in our opinion provides a good balance between scenarios with small and large sample sizes, moreover, analogous results have been found letting vary the value of T . Results are reported in Figure 4.

Once again, in all the circumstances the 99% confidence interval for the empirical coverage includes the target level of $1 - \alpha$, hence confirming the validity of the CP bands even for higher values of b . Moreover, one can

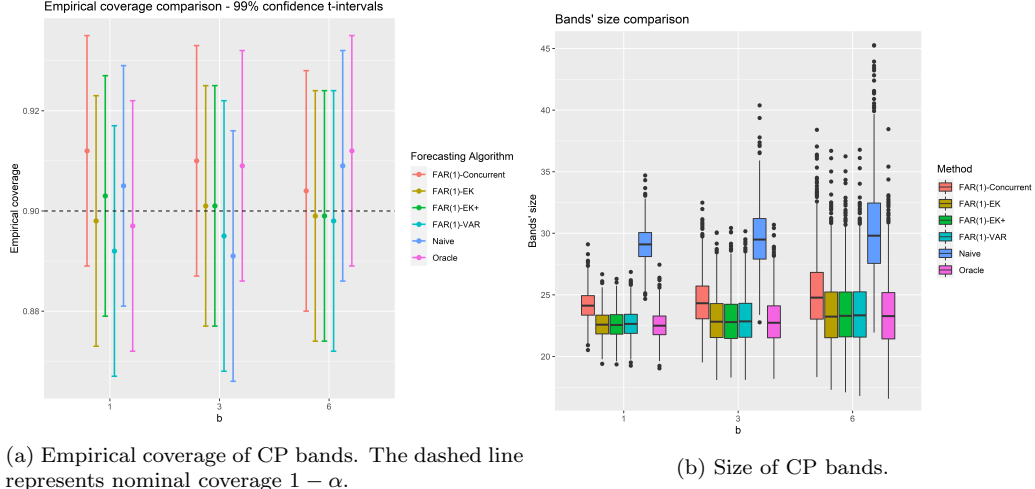


Figure 4: Results of second simulation study.

notice that, as already pointed out by [Diquigiovanni et al. \(2021a\)](#) in the one-dimensional functional setting, the band size tends to decrease when b decreases, thus providing more efficient prediction regions. We conjecture that this behaviour is related to the inverse proportionality between the blocking scheme size b and the dimension of the permutation family $|\Pi|$. A comparison of the different forecasting algorithms performances validates the consideration in Section 4.2.

5. Case Study: Forecasting Black Sea Level Anomaly

5.1. Dataset

In this section, we aim to illustrate the application potential of the proposed methodology on a proper case study. We will consider data from Copernicus, the European Union’s Earth observation program, which collects vast amounts of global data from satellites and ground-based, airborne, and seaborne measurement systems.

More specifically, we will analyze a data set from Copernicus Climate Change Service (C3S), a project operated by the European Center for Medium-Range Weather Forecasts (ECMWF), collecting daily sea level anomalies of the Black Sea in the last twenty years ([Mertz and Legeais 2018](#)). Sea level anomalies are measured as the height of water over the mean sea surface in a given time and region. Anomalies are computed with respect to a twenty-year

mean reference period (1993-2012). Satellite altimeters are used to estimate the sea level anomalies with a mapping algorithm dedicated to the Black Sea region. Observations are collected on a spatial raster, with a 0.125° resolution both on the longitude and on the latitude axis. Since observations are collected on a geoid, the domain actually lies on a two-dimensional manifold, however, because both longitude and latitude ranges are very small (14° and 7° respectively), we will ignore this detail and assume data to be observed on a bidimensional grid. The resulting lattice can hence be considered as the Cartesian product of a grid on the longitude axis made by $N_1 = 120$ points and a latitude grid of $N_2 = 56$ points. We will refer to (u_i, v_j) , with $i = 1, \dots, N_1$ and $j = 1, \dots, N_2$ as the point (i, j) -th of such two-dimensional mesh. Since the Black Sea does not have a rectangular shape, we will model such data as realization of random surfaces defined on the rectangle circumscribed to the perimeter of the sea, but identically equal to zero outside of it. As a consequence, being \mathcal{B} the set of points internal to the perimeter of the Black Sea, we slightly redefine the non conformity measure 3 to become:

$$\mathcal{A}(\{z_h : h \in \mathcal{I}_1\}, z) = \operatorname{ess\,sup}_{(u,v) \in [c,d] \times [e,f]} \mathcal{R}(u, v), \quad (25)$$

where $\mathcal{R}(u, v)$ is defined as:

$$\mathcal{R}(u, v) \begin{cases} \frac{|y(u,v) - g_{\mathcal{I}_1}(u,v; x_{T+1})|}{s_{\mathcal{I}_1}(u,v)}, & \text{if } (u, v) \in \mathcal{B} \\ 0 & \text{otherwise .} \end{cases} \quad (26)$$

Altimetry instruments give access to the sea surface height (SSH) above the reference ellipsoid (see Figure 5), which is calculated as the difference between the orbital altitude of the satellite and the measured altimetric distance of the satellite from the sea. Starting from this information, the Sea Level Anomaly (SLA) is defined as the anomaly of the signal around the Mean Sea Surface component (MSS), which is computed with respect to a 20-year reference period (1993-2012). Since we are settling the study in a functional data analysis framework, we will consider the time series $\{SLA_t\}$, without making explicit the dependence on the bivariate domain.

5.2. Data Preprocessing

If possible, one would preferably forecast directly the time series of Sea Level Anomalies (SLA_t). However, given the nature of the dataset, we expect anomalies to exhibit a strong seasonality as well as a linear trend (Cazenave

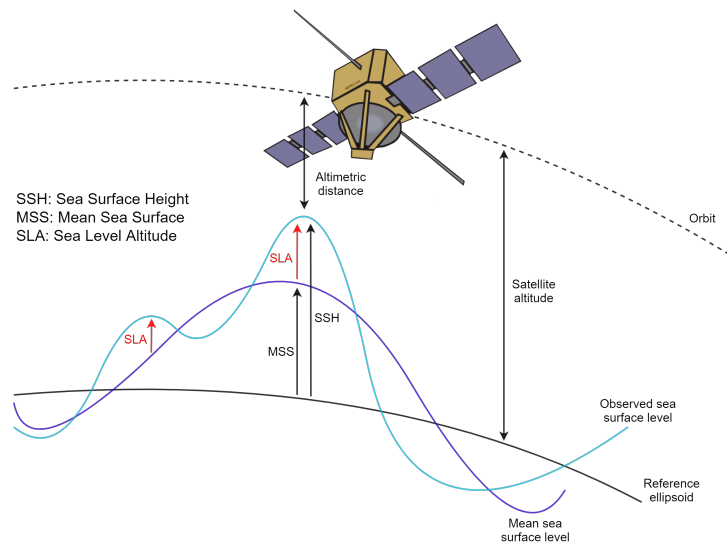


Figure 5: Data measurement process. The image is an author's replica of Figure 1 in Copernicus' [Product User Guide and Specification v2.4](#).

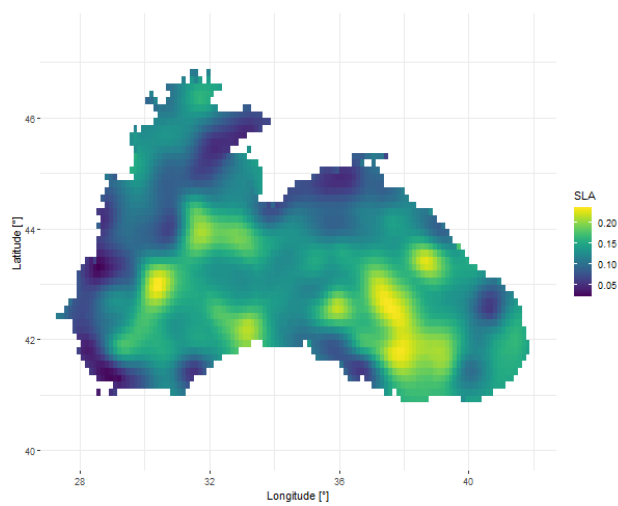


Figure 6: Raster representation of the Sea Level Anomaly (in meters) on 01/01/2018

et al. 2001). Moreover, both tide gauge and altimetry observations show that sea level trends in the Black Sea vary over time (Avsar et al. 2016). Tsimplis and Baker (2000) estimated a rise in the mean sea level of 2.2 mm/year from 1960 to the early 1990s, while long-track altimetry data indicate that sea level rose at a rate of 13.4 ± 0.11 mm/year over 1993–2008 (Ginzburg et al. 2011).

In order to further investigate this issue, we should proceed by testing the functional time series $\{SLA_t\}_t$ for stationarity. However, despite for one dimensional functional time series one could resort to the test proposed by Horváth et al. (2014), to the best of our knowledge an *ad-hoc* stationarity test for two-dimensional functional time series has still to be developed. For such reason, and aware of the limits of this approach, we will resort here to the analysis of stationarity of univariate time series $SLA_t(u_i, v_j)$, fixing some random locations (u_i, v_j) . We stress the fact that stationarity is indeed not necessary to obtain valid CP bands, but as proved by Chernozhukov et al. (2018), it is a sufficient condition to guarantee the first assumption of Theorem 1, that we would hence like to be satisfied.

By analyzing univariate time series $SLA_t(u_i, v_j)$ in fixed locations (u_i, v_j) , we acknowledge not negligible partial autocorrelation up to lag 2 or 3 depending on circumstances and the evident presence of a cyclical behaviour. Moreover, Augmented Dickey Fuller (ADF) stationarity test fails to reject the null hypothesis of unit root against the alternative one of a stationary process. As usually done in time series analysis, we proceed by differentiating $\{SLA_t\}_t$, hence considering the time series of first differences, $\{\Delta SLA_t\}_t$, defined as $\Delta SLA_t := SLA_t - SLA_{t-1}$. However, differentiated data still exhibit high partial autocorrelation for lags greater than one. A similar behaviour has also been found after a seasonal differentiation, where we employed as differentiation lag both a delay of 29 days, namely the moon phase cycle, and a lag of 365 days, coinciding with the Earth revolution time. Since we aim to eventually fit a Functional Autoregressive Process of order one, we proceed with a second differentiation, obtaining stationary time series with negligible partial autocorrelation for lags greater than one, as confirmed by ADF test and Partial Autocorrelation Function plots. Therefore, we will finally consider the time series of second differences $\{Y_t\}_t$, formally defined as:

$$Y_t := \Delta^2 SLA_t = (SLA_t - SLA_{t-1}) - (SLA_{t-1} - SLA_{t-2}) \quad (27)$$

We will forecast the differentiated time series Y_t , and obtain prediction

bands for it, using the methodology presented in Section 2. However, in order to provide a better insight into the prediction problem, we will then retrieve results pertaining to the original time series SLA_t . Specifically, we will apply the conformal machinery to the differentiated time series, calling \hat{Y}_{T+1} the forecasted function, and obtaining the prediction band for Y_{T+1} :

$$\mathcal{C}_{T,1-\alpha} := \left\{ y \in \mathbb{H} : y(u, v) \in \left[\hat{Y}_{T+1}(u, v) \pm k^s s_{\mathcal{I}_1}(u, v) \right] \forall (u, v) \right\}$$

Exploiting the fact that:

$$Y_{T+1}(u, v) \in \left[\hat{Y}_{T+1}(u, v) \pm k^s s_{\mathcal{I}_1}(u, v) \right] \quad \forall (u, v)$$

$$\Longleftrightarrow$$

$$SLA_{T+1}(u, v) \in \left[\hat{Y}_{T+1}(u, v) + 2SLA_T(u, v) - SLA_{T-1}(u, v) \pm k^s s_{\mathcal{I}_1}(u, v) \right] \forall (u, v)$$

we define the prediction band for SLA_{T+1} as:

$$\tilde{\mathcal{C}}_{T,1-\alpha} := \left\{ y \in \mathbb{H} : y(u, v) \in \left[\hat{Y}_{T+1}(u, v) + 2SLA_T(u, v) - SLA_{T-1}(u, v) \pm k^s s_{\mathcal{I}_1}(u, v) \right] \forall (u, v) \right\}$$

5.3. Study Design

The case study will employ a rolling estimation framework which recalculates the model parameters on a daily basis and consequently shifts and recomputes the entire training, calibration and test windows by 24 hours, as shown in Figure 7. As before, we will use a random split of data in the training and calibration sets, with split proportion equal to 50%. The significance level α is once again fixed equal to 0.1. For each of the 1000 days we aim to predict, we will build the corresponding prediction band based on the information provided by the last 99 days, thereby fixing $T = 99$. Choosing this value, indeed, provides accurate forecasts and thus small prediction bands, while maintaining reasonable computational times. The size of the blocking scheme will be fixed equal to 1, since, as motivated in Section 4.3, this choice produces the narrowest prediction bands, maintaining at the same time satisfactory performance in terms of empirical coverage. The rolling window will be shifted 1000 times, thus iterating for almost three years the forecasting of the next day based on the last T observations. More specifically, and to allow for reproducibility of subsequent results, we will consider a rolling window ranging from 01/01/2017 to 04/01/2020.

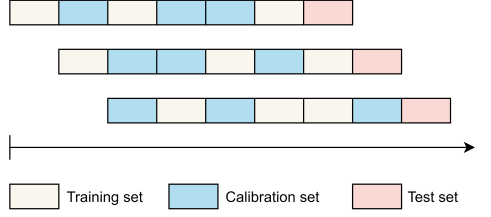


Figure 7: Example of the training-calibration-test split in a rolling window scenario.

The point predictors used throughout this application will be those described in Section 3. The number of Functional Principal Components is once again chosen by means of the cumulative proportion of variance criterion, setting the target percentage of variance value to 0.8.

For each shift of the rolling window and for each forecasting algorithm, we will check if SLA_{T+1} belongs to $\tilde{\mathcal{C}}_{T,1-\alpha}(x_{T+1})$, saving also the size of the corresponding prediction band. After having collected such results, we can calculate the average coverage, and use it to compare performances of the different point predictors in this scenario.

5.4. Results

In order to visualize results and show the potential applications of our method, we outline in Figure 12 the observed and forecast surfaces obtained for one of the day we aim to predict, as long as the lower and upper bounds defining the prediction band. For the sake of simplicity, we display only the results obtained using the FAR(1)-EK (16) estimator, since, as discussed below, it provides on average the narrowest prediction bands. In order to allow for a more insightful analysis, and to further investigate the evolution of such surfaces, we also implemented a dedicated [Shiny App](#) available online where results can be explored.

We report in Figure 15a the average coverage of the Conformal Prediction bands obtained across 1000 predictions. As in Section 4, we pair such quantity with a 99% confidence interval. Notice that in this case the confidence interval may be biased, due to the inevitable correlation between data used to construct it, however, we still decided to include it in order to assess the dispersion of the average coverage around the mean. Coherently with the results of the simulation study, we can appreciate that in all cases the prediction bands capture the observed surface y_{T+1} approximately $(1 - \alpha)\%$ of the times, regardless of the forecasting algorithm used.

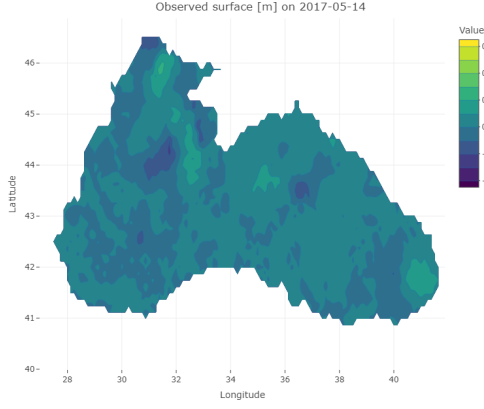


Figure 8: Observed Surface

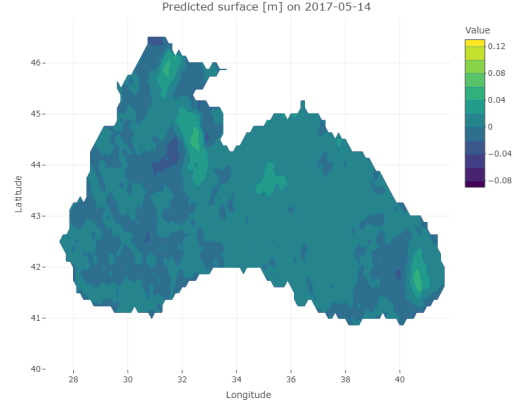


Figure 9: Predicted Surface

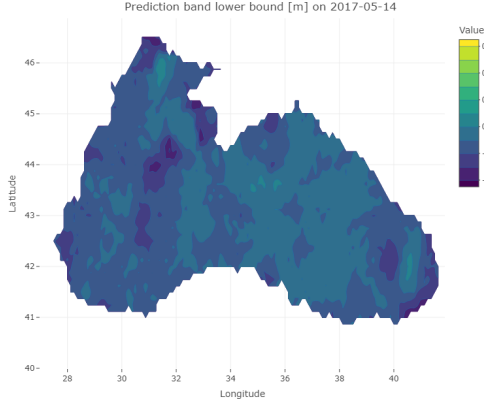


Figure 10: Prediction Band Lower Bound

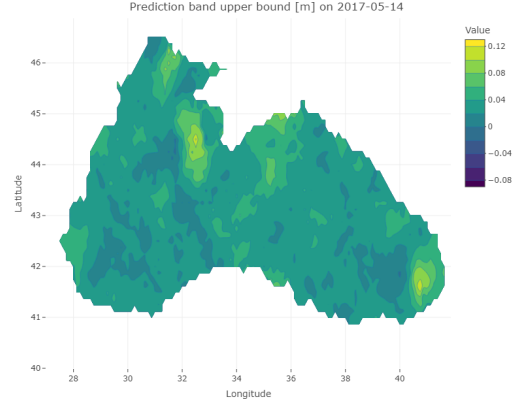


Figure 11: Prediction Band Upper Bound

Figure 12: Observed surface, predicted surface, prediction band lower bound, prediction band upper bound on 14/05/2017. Results are obtained using a sample size T equal to 99, $b = 1$, $l = 48$, $\alpha = 0.1$. The employed forecasting algorithm $g_{\mathcal{I}_1}$ is FAR(1)-EK (16).

For what concerns the size of the prediction bands, the Naive predictor produces by far the widest ones (see [Figure 15b](#)), and, this fact does not reflect in a greater coverage compared to the other methods. On the other hand, prediction bands obtained with forecasting algorithms modelling the autoregressive structure provide narrower prediction regions. Among these, we can see that the non-concurrent FAR(1) is the most performing one, despite the way in which it is estimated (namely with FAR(1)-EK, FAR(1)-EK+ or FAR(1)-VAR). Nevertheless, also the concurrent FAR(1) model provides very tight prediction bands, almost comparable with the ones produced by the non-concurrent prediction algorithm.

We are also interested in analyzing the *pointwise* properties of CP bands in this scenario. Therefore, we display in [Figure 13](#) a map of the pointwise coverage of the prediction bands, obtained using FAR(1)-EK. We can appreciate, as expected, a high empirical coverage across the entire domain, emphasizing once again the peculiarity of our approach, which guarantees global coverage of the prediction surfaces, reflected by an obvious pointwise coverage higher than the global one. We report in [Figure 13](#) also the average width of such bands, which denotes a peculiar pattern, probably due to data collection routines. Indeed, we can see from [Figure 14b](#), that a similar behaviour observed in the map of pointwise width can be found by plotting the standard deviation of original data. This is coherent with the employed CP framework, since the size of prediction bands depends on the amplitude of the functional standard deviation.

In conclusion, the study case confirms the validity of our procedure and proves how a FAR(1) model significantly improves the predictive efficiency even in this more complex scenario. We conjecture that the accuracy of the forecast surface (and thus the efficiency of the resulting CP bands) may be further enhanced by taking into consideration a more refined predictor.

6. Conclusions and Further Developments

In this work, we proposed a mathematical framework for probabilistic forecasting of two-dimensional functional time series. Moving from the work of [Chernozhukov et al. \(2018\)](#) and [Diquigiovanni et al. \(2021a\)](#), we presented in [Section 3](#) a randomization inference procedure, called Conformal Prediction, adapting it to our specific setting, and thus allowing for uncertainty quantification. Given the novelty of the subject, we have also extended classical forecasting procedures from the one-dimensional functional framework. In

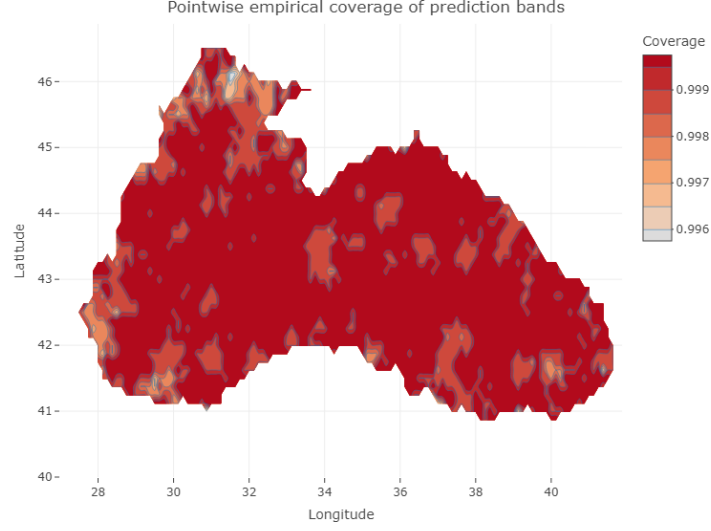


Figure 13: Pointwise coverage of the prediction bands across the domain, obtained by counting the number of times that each point falls between prediction bands, and dividing by the total number of time steps in the rolling window framework.

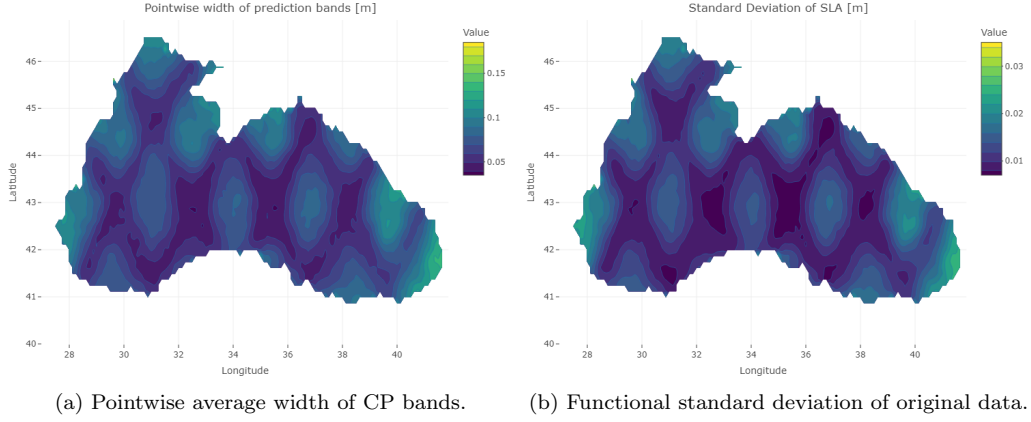


Figure 14: Comparison between CP bands' pointwise average width map and functional standard deviation of original data. The figure on the right denotes a peculiar pattern in the data collection process, which is retrieved in the left panel, due to the choice of using the standard deviation as a modulation function in the CP framework.

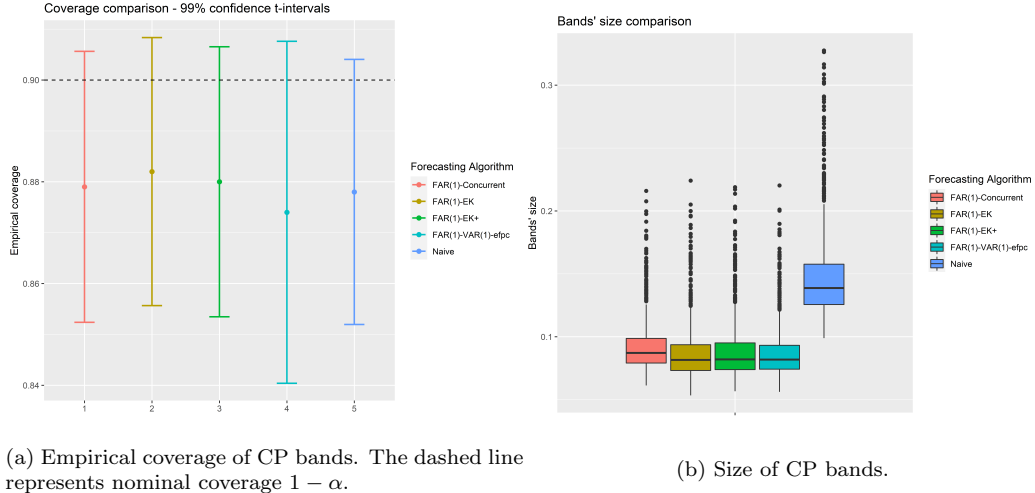


Figure 15: Results of the forecasting procedure in a rolling window setting. All the methods produce prediction bands with average coverages close to the nominal one. For what concerns predictive efficiency, the naive predictor produces the widest bands, whereas the other methods produce instead more efficient bands, with sizes similar to each other.

particular, we have focused on the non-concurrent Functional Autoregressive process of order one, which represents the state of the art of functional time series modelling, thereby proposing different estimation techniques. Whereas Theorem 1 provides theoretical performance guarantees of the uncertainty quantification algorithm, we were interested in verifying empirical properties of CP bands, and, at the same time, testing and comparing different forecasting algorithms in terms of the resulting prediction regions. We proved the strength of the proposed method through a proper simulation study, emphasizing the advantages of using a correctly specified forecasting model. We have finally applied the proposed technique to a real case study, employing a novel time series dataset, which consists of daily observations of Sea Anomaly Level over the Black Sea during the last 20 years. Empirical results proved the validity of our approach even on non-synthetic data.

Throughout this work, we modeled time series of surfaces as two-dimensional functional time series. This approach is very appealing, since it permits to embed the analysis in a Hilbert space, thus providing a solid mathematical framework. An interesting further development could be to exploit more advanced Machine Learning forecasting algorithms in the prediction pipeline. For instance, given the temporal dependence of our data, one might predict

the next realization of the time series through a Recurrent Neural Network (RNN) or one of its improved versions, such as Long Short Term Memory (LSTM) or Gated Recurrent Units (GRU). Moreover, since surfaces can be represented as bidimensional images, one may also consider adding convolutional layers to the network. We stress the fact that this approach is not antithetical to our work. In fact, given the high flexibility of the uncertainty quantification technique employed, namely Conformal Prediction, we would just have to substitute the point predictor $g_{\mathcal{I}_1}$ with a user-defined neural network, while keeping the rest of the procedure unchanged, in order to pair the forecasted surfaces with probabilistic prediction bands. As shown in the simulation study, we expect that an improvement in the quality of the point predictor will result in narrower and thus more efficient prediction bands.

Acknowledgments

This work has been partially supported by ACCORDO Attuativo ASI-POLIMI “Attività di Ricerca e Innovazione” n. 2018-5-HH.0, collaboration agreement between the Italian Space Agency and Politecnico di Milano. M.F. acknowledges the support of the JRC Centre of Advanced Studies CSS4P - “Computational Social Science for Policy”

References

- Aue, A., Norinho, D., Hörmann, S., 2012. On the prediction of stationary functional time series. *Journal of the American Statistical Association* 110. doi:[10.1080/01621459.2014.909317](https://doi.org/10.1080/01621459.2014.909317).
- Avsar, N.B., Jin, S., Kutoglu, H., Gurbuz, G., 2016. Sea level change along the black sea coast from satellite altimetry, tide gauge and gps observations. *Geodesy and Geodynamics* 7, 50–55. doi:<https://doi.org/10.1016/j.geog.2016.03.005>. special Issue: GNSS Applications in Geodesy and Geodynamics.
- Balasubramanian, S., Karrh, J., Patwardhan, H., 2006. Audience response to product placements: An integrative framework and future research agenda. *Journal of Advertising* 35, 115–141. doi:[10.2753/JOA0091-3367350308](https://doi.org/10.2753/JOA0091-3367350308).
- Bosq, D., 2000. *Linear Processes in Function Spaces*. Springer New York. URL: <https://link.springer.com/book/10.1007/978-1-4612-1154-9>.

- Cazenave, A., Cabanes, C., Dominh, K., Mangiarotti, S., 2001. Recent sea level change in the mediterranean sea revealed by topex/poseidon satellite altimetry. *Geophysical Research Letters* 28, 1607–1610. doi:<https://doi.org/10.1029/2000GL012628>.
- Chernozhukov, V., Wüthrich, K., Yinchu, Z., 2018. Exact and robust conformal inference methods for predictive machine learning with dependent data, in: Bubeck, S., Perchet, V., Rigollet, P. (Eds.), *Proceedings of the 31st Conference On Learning Theory*, PMLR. pp. 732–749. URL: <https://proceedings.mlr.press/v75/chernozhukov18a.html>.
- Didericksen, D., Kokoszka, P., Zhang, X., 2010. Empirical properties of forecasts with the functional autoregressive model. *Computnl Statist.* 27, 285–298. doi:[10.1007/s00180-011-0256-2](https://doi.org/10.1007/s00180-011-0256-2).
- Diquigiovanni, J., Fontana, M., Vantini, S., 2021a. Distribution-free prediction bands for multivariate functional time series: an application to the italian gas market. [arXiv:2107.00527](https://arxiv.org/abs/2107.00527).
- Diquigiovanni, J., Fontana, M., Vantini, S., 2021b. The importance of being a band: Finite-sample exact distribution-free prediction sets for functional data. [arXiv:2102.06746](https://arxiv.org/abs/2102.06746).
- Fontana, M., Zeni, G., Vantini, S., 2022. Conformal prediction: a unified review of theory and new challenges. *Bernoulli* To appear.
- Gammerman, A., Vovk, V., Vapnik, V., 1998. Learning by transduction, in: *Proceedings of the Fourteenth Conference on Uncertainty in Artificial Intelligence*, Morgan Kaufmann Publishers Inc., San Francisco, CA, USA. p. 148–155.
- Gervini, D., 2010. Retracted: The functional singular value decomposition for bivariate stochastic processes. *Computational Statistics and Data Analysis* 54, 163–172. doi:<https://doi.org/10.1016/j.csda.2009.07.024>.
- Ginzburg, A.I., Kostianoy, A.G., Sheremet, N.A., Lebedev, S.A., 2011. Satellite altimetry applications in the black sea, in: Vignudelli, S., Kostianoy, A.G., Cipollini, P., Benveniste, J. (Eds.), *Coastal Altimetry*, Springer Berlin Heidelberg, Berlin, Heidelberg. pp. 367–387. doi:[10.1007/978-3-642-12796-0_14](https://doi.org/10.1007/978-3-642-12796-0_14).

- Horváth, L., Kokoszka, P., 2012. Inference for Functional Data with Applications. Springer Series in Statistics, Springer New York. URL: https://books.google.it/books?id=0VezLB__ZpYC.
- Horváth, L., Kokoszka, P., Rice, G., 2014. Testing stationarity of functional time series. *Journal of Econometrics* 179, 66–82. doi:<https://doi.org/10.1016/j.jeconom.2013.11.002>.
- Hyndman, R., Shang, H.L., 2009. Functional time series forecasting. *Journal of the Korean Statistical Society* 38. doi:[10.1016/j.jkss.2009.06.002](https://doi.org/10.1016/j.jkss.2009.06.002).
- Hörmann, S., Kokoszka, P., 2010. Weakly dependent functional data. *The Annals of Statistics* 38, 1845 – 1884. URL: <https://doi.org/10.1214/09-AOS768>, doi:[10.1214/09-AOS768](https://doi.org/10.1214/09-AOS768).
- Hörmann, S., Łukasz, K., 2017. freqdom.fda: Functional time series: Dynamic functional principal components. URL: <https://cran.r-project.org/web/packages/freqdom.fda/index.html>.
- Ivanescu, Andrada, 2013. A note on bivariate smoothing for two-dimensional functional data. *International Journal of Statistics and Probability* 2. doi:[10.5539/ijsp.v2n2p102](https://doi.org/10.5539/ijsp.v2n2p102).
- Kargin, V., Onatski, A., 2005. Curve forecasting by functional autoregression. *Journal of Multivariate Analysis* 99, 2508–2526. doi:[10.1016/j.jmva.2008.03.001](https://doi.org/10.1016/j.jmva.2008.03.001).
- Kath, C., Ziel, F., 2021. Conformal prediction interval estimation and applications to day-ahead and intraday power markets. *International Journal of Forecasting* 37, 777–799. URL: <http://dx.doi.org/10.1016/j.ijforecast.2020.09.006>, doi:[10.1016/j.ijforecast.2020.09.006](https://doi.org/10.1016/j.ijforecast.2020.09.006).
- Lei, J., Rinaldo, A., Wasserman, L., 2015. A conformal prediction approach to explore functional data. *Annals of Mathematics and Artificial Intelligence* 74, 29–43. doi:[10.1007/s10472-013-9366-6](https://doi.org/10.1007/s10472-013-9366-6).
- López-Pintado, S., Romo, J., 2009. On the concept of depth for functional data. *Journal of the American Statistical Association* 104, 718–734. doi:[10.1198/jasa.2009.0108](https://doi.org/10.1198/jasa.2009.0108).

- Mertz, F., Legeais, J.F., 2018. Sea level daily gridded data from satellite observations for the black sea from 1993 to 2020. URL: <https://cds.climate.copernicus.eu/cdsapp#!/dataset/satellite-sea-level-black-sea?tab=overview>.
- Papadopoulos, H., Proedrou, K., Vovk, V., Gammernan, A., 2002. Inductive confidence machines for regression, in: Elomaa, T., Mannila, H., Toivonen, H. (Eds.), Machine Learning: ECML 2002, Springer Berlin Heidelberg, Berlin, Heidelberg. pp. 345–356. URL: https://doi.org/10.1007/3-540-36755-1_29.
- Porro-Muñoz, D., Mata, F.J.S., Hernández, N., Bustamante, I.T., 2014. Functional data analysis as an alternative for the automatic biometric image recognition: Iris application. *Computación y Sistemas* 18, 111–121. doi:[10.13053/CyS-18-1-2014-022](https://doi.org/10.13053/CyS-18-1-2014-022).
- R Core Team, 2020. R: A Language and Environment for Statistical Computing. R Foundation for Statistical Computing. Vienna, Austria. URL: <https://www.R-project.org/>.
- Rakê, L.L., 2010. 2D Functional Data Analysis, with applications to image analysis. Master’s thesis. Statistics Department of Mathematical Sciences, Faculty of Science, University of Copenhagen.
- Ramsay, J., Silverman, B., 2005. Functional Data Analysis. Springer Series in Statistics, Springer. URL: https://books.google.it/books?id=mU3dop5wY_4C.
- Rossini, J., Canale, A., 2018. Quantifying prediction uncertainty for functional-and-scalar to functional autoregressive models under shape constraints. *Journal of Multivariate Analysis* 170, 221–231. doi:[10.1016/j.jmva.2018.10.007](https://doi.org/10.1016/j.jmva.2018.10.007).
- Solari, A., Djordjilović, V., 2021. Multi split conformal prediction. *arXiv:2103.00627*.
- Tsimplis, M.N., Baker, T.F., 2000. Sea level drop in the mediterranean sea: An indicator of deep water salinity and temperature changes? *Geophysical Research Letters* 27, 1731–1734. doi:<https://doi.org/10.1029/1999GL007004>.

- Vovk, V., Gammerman, A., Shafer, G., 2005. Algorithmic Learning in a Random World. Springer New York. URL: <https://link.springer.com/book/10.1007/b106715>.
- Wisniewski, W., Lindsay, D., Lindsay, S., 2020. Application of conformal prediction interval estimations to market makers’ net positions, in: Gammerman, A., Vovk, V., Luo, Z., Smirnov, E., Cherubin, G. (Eds.), Proceedings of the Ninth Symposium on Conformal and Probabilistic Prediction and Applications, PMLR. pp. 285–301. URL: <https://proceedings.mlr.press/v128/wisniewski20a.html>.
- Zhou, L., Pan, H., 2014. Principal component analysis of two-dimensional functional data. Journal of Computational and Graphical Statistics 23, 779–801. doi:[10.1080/10618600.2013.827986](https://doi.org/10.1080/10618600.2013.827986).

Appendix A. Split ratio and type of split

The choice of the split ratio is non-trivial and has motivated discussion in the statistical community. Including more data in the training set improves the estimation of the point predictor $\hat{g}_{\mathcal{I}_1}$. At the same time, having a few data points in the calibration set produces a very rough p-value function (7), resulting in potential greater actual coverage with respect to the nominal one. This trade-off problem is enhanced in the time series context, in which one would like to have both training and calibration sets as large as possible, since asymptotic validity is guaranteed when both l and m go to infinity. Throughout this work, the training-calibration ratio is fixed equal to 50%-50%, as commonly suggested in literature. Moreover, we stress the fact that the split is random. This clearly introduces variability in the procedure since results depend on the particular division of data. We acknowledge a recent advancement in this direction, namely Multi Split Conformal Prediction (Solarì and Djordjilović 2021), which aggregates single split CP intervals across multiple splits.

Another interesting question regarding the type of split comes up in the time series context. Due to the lack of exchangeability, two different subdivisions are possible in this framework. A first choice could consist in a sequential division of data, where the split point is no longer random, but is a result of the training-calibration proportion (see A.16a). Wisniewski et al. (2020) applied this scheme in a rolling window fashion to forecast Market Makers’ Net Positions. While this choice may seem more consistent in the

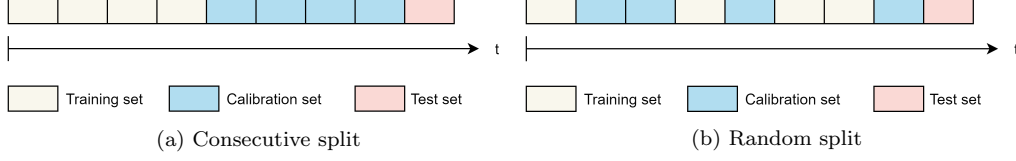


Figure A.16: Possible types of split with $T = 8$, $m = l = 4$.

presence of temporal dependence, since it does not split subsequent observations in two different sets, it may lead to very biased results if the training size m is very small or if data present a different trend or seasonal component in the training and calibration sets. The interested reader may refer to [Kath and Ziel \(2021\)](#) for a more comprehensive discussion on this topic. All in all, in order to make the model more robust, we preferred to split data randomly, as reported in [A.16b](#).

Appendix B. FAR(1) estimation and adaptation to CP

Hereafter, we will assume $\{Y_t\}_{t=1}^T \subset \mathcal{L}^4(\Omega, \mathcal{F}, \mathbb{P})$ and consider only zero-mean stationary time series. The covariance operator $\Gamma_0 : \mathbb{H} \rightarrow \mathbb{H}$ and the lag-1 autocovariance operator Γ_1 can thus be defined as:

$$\Gamma_0 x = \mathbb{E}[\langle Y_t, x \rangle Y_t] \quad \forall x \in \mathbb{H} \quad (\text{B.1})$$

$$\Gamma_1 x = \mathbb{E}[\langle Y_t, x \rangle Y_{t+1}] \quad \forall x \in \mathbb{H} \quad (\text{B.2})$$

Extending the work of [Horváth and Kokoszka \(2012\)](#) to a different functional space, we can derive the following estimators for such operators:

$$\hat{\Gamma}_0 x = \frac{1}{T} \sum_{t=1}^T \langle Y_t, x \rangle Y_t \quad \forall x \in \mathbb{H} \quad (\text{B.3})$$

$$\hat{\Gamma}_1 x = \frac{1}{T-1} \sum_{t=1}^{T-1} \langle Y_t, x \rangle Y_{t+1} \quad \forall x \in \mathbb{H} \quad (\text{B.4})$$

Under rather general weak dependence assumptions these estimators are \sqrt{n} -consistent. One may, for example, adopt the concept of \mathcal{L}^p - m -approximability introduced in [Hörmann and Kokoszka \(2010\)](#) to prove that $\mathbb{E}[|\hat{\Gamma}_0 - \Gamma_0|^2] = \mathcal{O}(n^{-1})$, where $\|\cdot\|$ is the classical operatorial norm: $\|F\| := \sup_{\|x\|_{\mathbb{H}}=1} \|Fx\|_{\mathbb{H}}$ for any linear bounded operator $F : \mathbb{H} \rightarrow \mathbb{H}$.

In order to derive estimator (16) of the FAR(1), we will consider first the following operatorial equation:

$$\Gamma_1 = \Psi \Gamma_0 \quad (\text{B.5})$$

A natural idea may consist in computing estimators $\hat{\Gamma}_0, \hat{\Gamma}_1$ from historical data and defining then $\hat{\Psi} = \hat{\Gamma}_0 \hat{\Gamma}_0^{-1}$. Unfortunately, the inverse operator Γ_0^{-1} is unbounded on \mathbb{H} (Horváth and Kokoszka 2012), however, thanks to Γ_0 being a symmetric, compact, positive-definite operator, one can exploit its spectral decomposition to introduce a pseudo-inverse operator $\Gamma_{0,M}^{-1}$, defined as:

$$\Gamma_{0,M}^{-1}x = \sum_{j=1}^M \lambda_j^{-1} \langle x, \xi_j \rangle \xi_j \quad \forall x \in \mathbb{H} \quad (\text{B.6})$$

where ξ_1, \dots, ξ_M are the first M normalized functional principal components (FPC's), $\lambda_1, \dots, \lambda_M$ are the corresponding eigenvalues and $\langle x, \xi_1 \rangle, \dots, \langle x, \xi_M \rangle$ are the scores of x along the FPC's. We formally define ξ_i and λ_i as eigenfunctions and eigenvalues that solve the functional equation:

$$\Gamma_0 \xi_i = \lambda_i \xi_i \quad i = 1, \dots, M \quad (\text{B.7})$$

We can now combine (B.5) and (B.6), plugging in estimated eigenfunctions and eigenvalues and calling $\hat{\Gamma}_{0,M}^{-1}$ the resulting estimator of $\Gamma_{0,M}^{-1}$, to finally derive:

$$\hat{\Psi}_M = \hat{\Gamma}_1 \hat{\Gamma}_{0,M}^{-1} x \quad (\text{B.8})$$

$$\hat{\Psi}_M x = \frac{1}{T-1} \sum_{i,j=1}^M \sum_{t=1}^T \hat{\lambda}_j \langle x, \hat{\xi}_j \rangle \langle Y_{t-1}, \hat{\xi}_j \rangle \langle Y_t, \hat{\xi}_i \rangle \hat{\xi}_i \quad \forall x \in \mathbb{H} \quad (\text{B.9})$$

Notice that the operator $\hat{\Gamma}_{0,M}^{-1}$ is bounded on \mathbb{H} if $\hat{\lambda}_j$ are strictly greater than zero for $j = 1, \dots, M$. Nevertheless, even if such condition is met, in practice one should cautiously select the number of principal components M , because very small eigenvalues will result in very high reciprocals $\hat{\lambda}_j^{-1}$, providing in practice unbounded estimates of $\Gamma_{0,M}^{-1}$. Such observation motivated Didericksen et al. (2010) to add a positive baseline to the estimated eigenvalues $\hat{\lambda}_j$. This small modification improves the estimation of the operator Ψ , and most importantly, contributes to weaken the dependency of $\hat{\Psi}_M$ on M .

We now aim to adapt the previous estimator (B.9) to the conformal inference setting. The goal is to accommodate the forecasting algorithm in order to estimate the point predictor $g_{\mathcal{I}_1}$ from the training set only.

As a preliminary step, given that the FAR(1) model has been presented for mean-centered data, one has to estimate the mean function $\hat{\mu}_{\mathcal{I}_1}$ from the training set only and consequently center all the observations in the training and calibration set around $\hat{\mu}_{\mathcal{I}_1}$. If the sample size at disposal is sufficiently large and if the stationarity assumption is fulfilled, it should make no great difference to estimate the population function μ with the sample mean $\hat{\mu} = \frac{1}{T} \sum_{t=1}^T Y_t$ or with its restriction on the training set $\hat{\mu}_{\mathcal{I}_1} = \frac{1}{m} \sum_{t \in \mathcal{I}_1} Y_t$. Another fundamental step is the estimation of functional principal components. Since in the CP framework we are allowed to use only the information from the training set in order to compute $\hat{\xi}_1, \dots, \hat{\xi}_M$, it is then natural to employ only training data $\{z_h : h \in \mathcal{I}_1\}$ in such estimation routine.

In order to obtain estimator $\hat{\Psi}_M$ (16), one has to compute $\hat{\Gamma}_1$ and $\hat{\Gamma}_{0,M}^{-1}$ from the training set. While the computation of the sample pseudo-inverse of the autocovariance estimator is straightforward:

$$\hat{\Gamma}_{0,M}^{-1}x = \frac{1}{m} \sum_{j=1}^M \lambda_j \langle x, \hat{\xi}_j \rangle \hat{\xi}_j \quad \forall x \in \mathbb{H} \quad (\text{B.10})$$

the CP counterpart of $\hat{\Gamma}_1$ is more delicate and requires further discussion. Recall indeed that the classical estimator for the lag-1 autocovariance operator from Y_1, \dots, Y_T is:

$$\hat{\Gamma}_1 x = \frac{1}{T-1} \sum_{t=1}^{T-1} \langle Y_t, x \rangle y_{t+1} = \quad (\text{B.11})$$

$$= \frac{1}{T-1} \sum_{t=2}^T \langle Y_{t-1}, x \rangle Y_t \quad (\text{B.12})$$

In the CP setting, however, we could define three different estimators for Γ_1 :

$$\hat{\Gamma}_1 x = \frac{1}{m-1} \sum_{t \in \mathcal{I}_1[1:m-1]} \langle Y_t, x \rangle Y_{t+1} \quad (\text{B.13})$$

$$\hat{\Gamma}_1 x = \frac{1}{m-1} \sum_{t \in \mathcal{I}_1[2:m]} \langle Y_{t-1}, x \rangle Y_t \quad (\text{B.14})$$

$$\hat{\Gamma}_1 x = \frac{1}{m} \sum_{t \in \mathcal{I}_1} \langle Y_{t-1}, x \rangle Y_t \quad (\text{B.15})$$

where $x \in \mathbb{H}$ and $\mathcal{I}_1[i : j]$ contains the indices from the i -th to the j -th element of \mathcal{I}_1 . Notice that the three estimators differ because if $t \in \mathcal{I}_1$, we have no assurance that $\{t-1\} \in \mathcal{I}_1$ or even $\{t+1\} \in \mathcal{I}_1$. We stress also the fact that the third operator is well-defined only if we reserve a burn-in set of length 1 at the front of the time series, in such a way that, if $\{2\} \in \mathcal{I}_1$, we can still compute the estimator. Among the three options, we will prefer the third one (B.15), since it averages over a larger set. One may also argue that such estimators are not coherent with the CP setting, since they are inevitably based on data from the calibration set. However, as mentioned before, we are considering the time series of *regression pairs* $Z_t = (X_t, Y_t)$, $t = 1, \dots, T$. The key consideration is that, according to the FAR(1) model, we use as regressors the lagged version of the time series, namely $X_t = Y_{t-1}$ and the regression couples becomes $Z_t = (Y_{t-1}, Y_t)$, for each $t = 1, \dots, T$. From this perspective, one could rephrase the definition of the sample covariance operator by making explicit its dependence from the regressor X_t instead of Y_{t-1} :

$$\hat{\Gamma}_1 x = \frac{1}{m-1} \sum_{t \in \mathcal{I}_1} \langle Y_{t-1}, x \rangle Y_t = \quad (\text{B.16})$$

$$= \frac{1}{m} \sum_{t \in \mathcal{I}_1} \langle X_t, x \rangle Y_t \quad (\text{B.17})$$

It is then straightforward to derive the estimator $\hat{\Psi}_{M, \mathcal{I}_1}$:

$$\hat{\Psi}_{M, \mathcal{I}_1} x = \frac{1}{m} \sum_{i,j=1}^M \sum_{t \in \mathcal{I}_1} \hat{\lambda}_j \langle x, \hat{\xi}_j \rangle \langle Y_{t-1}, \hat{\xi}_j \rangle \langle Y_t, \hat{\xi}_i \rangle \hat{\xi}_i = \quad (\text{B.18})$$

$$= \frac{1}{m} \sum_{i,j=1}^M \sum_{t \in \mathcal{I}_1} \hat{\lambda}_j \langle x, \hat{\xi}_j \rangle \langle X_t, \hat{\xi}_j \rangle \langle Y_t, \hat{\xi}_i \rangle \hat{\xi}_i \quad \forall x \in \mathbb{H} \quad (\text{B.19})$$

The point predictor finally becomes:

$$\hat{Y}_{T+1} = g_{\mathcal{I}_1}(u, v; X_{T+1}) = (\hat{\Psi}_{M, \mathcal{I}_1} X_{T+1})(u, v) = (\hat{\Psi}_{M, \mathcal{I}_1} Y_T)(u, v) \quad (\text{B.20})$$

In order to compute (B.19), it is first mandatory to project the calibration set onto the EPFC's in order to compute the scores $\langle X_h, \hat{\xi}_j \rangle$ for $h \in \mathcal{I}_2$. Notice that, in the non-Conformal setting, such step comes for free when performing FPCA. In the CP context, however, EPFC's are computed from the training set only, therefore, in order to access the scores of the calibration set, one needs to explicitly add this projection step.

Appendix C. FPCA for Two-Dimensional Functional Data

A fundamental aspect in the design of many forecasting algorithms is the estimation of functional principal components (FPC's) $\{\xi_i\}_{i \in \mathbb{N}}$. We define FPC's as functions $\xi_i \in \mathcal{L}^2([c, d] \times [e, f])$ solving the functional equation:

$$\Gamma_0 \xi = \lambda \xi \quad (\text{C.1})$$

In practice, we can only estimate the first $M \in \mathbb{N}$ eigenfunctions, implicitly performing dimensionality reduction. The choice of M is non-trivial and depends on the application framework. Whereas [Kargin and Onatski \(2005\)](#) suggested selecting it in a cross-validation setting, [Aue et al. \(2012\)](#) proposed a fully automatic criterion for choosing the number of principal components in terms of predictive performances. Plugging in the estimator of Γ_0 , we define estimated eigenfunctions and eigenvalues as solutions of:

$$\hat{\Gamma}_0 \hat{\xi} = \hat{\lambda} \hat{\xi} \quad (\text{C.2})$$

On a theoretical point of view, we would like to guarantee that population eigenfunctions can be consistently estimated by empirical eigenfunctions even in the non-iid framework of Functional Time Series. We refer to Theorem 16.2 in [Horváth and Kokoszka \(2012\)](#), which provides asymptotic arguments for such question.

The following subsections are dedicated to the estimation of eigenfunctions and eigenvalue in the two-dimensional functional case. Extending the work of [Ramsay and Silverman \(2005\)](#), we present two different estimation procedures, based respectively on a discretization of the functions to a fine grid and on a linear expansion of data on a finite set of basis functions.

Among the two alternatives, we would resort to the function discretization. Indeed, such choice does not require the selection of a specific type of basis and not even the number of basis to employ, which are not trivial problem-dependent questions. Moreover, notice that also the discretization procedure can be seen as a particular case of the basis expansion, using as basis system indicator functions on the grid points. Furthermore, in the subsequent, [Appendix C.3](#) we will demonstrate with a simulation study that there is no significant evidence to prefer one method against the other in terms of estimation quality.

We want to stress the fact that our methodology for FPCA is general, it works for two-dimensional functional data regardless of the presence of temporary dependence between observations. Not modeling the serial dependence structure will not invalidate the PCA procedure, but we still have to require that the dynamic is stationary in order for the covariance estimation to make sense and thus to provide meaningful estimates.

Appendix C.1. Grid Discretization

Consider a grid discretization $\{u_i\}_{i=1,\dots,N_1}$ of $[c, d]$ and $\{v_j\}_{j=1,\dots,N_2}$ of $[e, f]$, let $\omega_1 = \frac{1}{N_1}$, $\omega_2 = \frac{1}{N_2}$. For any point (u_i, v_j) of the discretized grid, the lhs of the functional eigenequation (C.2) can be rewritten as:

$$\hat{\Gamma}_0 \hat{\xi}(u_i, v_j) = \int_c^d \int_e^f \hat{\gamma}_0(u_i, v_j; w, z) \hat{\xi}(w, z) dw dz \approx \quad (C.3)$$

$$\approx \omega_1 \sum_{l=1}^{N_1} \int_e^f \hat{\gamma}_0(u_i, v_j; u_l, z) \hat{\xi}(u_l, z) dz \approx \quad (C.4)$$

$$\approx \omega_1 \omega_2 \sum_{l=1}^{N_1} \sum_{m=1}^{N_2} \hat{\gamma}_0(u_i, v_j; u_l, v_m) \hat{\xi}(u_l, v_m) \quad (C.5)$$

By defining $N := N_1 N_2$ and introducing a bijection $\zeta : \{1, \dots, N_1\} \times \{1, \dots, N_2\} \rightarrow \{1, \dots, N\}$, we can vectorize the two-dimensional grid. Therefore, we can group observed data into a bidimensional matrix, and proceed with a usual multivariate analysis. Let $\mathbb{Y} \in \mathbb{R}^{T \times N}$ be defined as $\mathbb{Y}[t, \zeta(i, j)] = y_t(u_i, v_j)$. We hence introduce the estimated variance-covariance matrix of the just defined multivariate dataset: $\hat{\Gamma}_0 \in \mathbb{R}^{N \times N}$, $\hat{\Gamma}_0 = \frac{1}{T} \mathbb{Y}^T \mathbb{Y}$. Notice that $\hat{\Gamma}_0[\zeta(i, j), \zeta(l, m)] = \hat{\gamma}_0(u_i, v_j; u_l, v_m)$. Let also $\hat{\xi} \in \mathbb{R}^N$, $\hat{\xi}[\zeta(i, j)] = \hat{\xi}(u_i, v_j)$. The eigenequation can thus be rewritten in the following matricial form:

$$\omega_1 \omega_2 \hat{\Gamma}_0 \hat{\xi} = \hat{\lambda} \hat{\xi} \quad (C.6)$$

It is then straightforward to find the eigenvalues ρ and eigenvectors $\boldsymbol{\theta}$ of the matrix $\mathbf{\Gamma}_0$ and to derive $\hat{\lambda} = \omega_1 \omega_2 \rho$ and $\hat{\boldsymbol{\xi}} = \omega_1^{-1/2} \omega_2^{-1/2} \boldsymbol{\theta}$. Finally, to obtain an approximate eigenfunction ξ from discrete values $\hat{\boldsymbol{\xi}}$, we can use any convenient interpolation method.

Appendix C.2. Basis Expansion

Let $\{g_i\}_{i \in \mathbb{N}}$ be a basis system for $\mathcal{L}^2([c, d])$ and $\{h_j\}_{j \in \mathbb{N}}$ a basis system for $\mathcal{L}^2([e, f])$. Consider now the tensor product basis $\{g_i \otimes h_j\}_{i,j}$, where $g_i \otimes h_j = g_i h_j$. Unfortunately, the space spanned by the tensor product basis is a proper subset of $\mathbb{H} = \mathcal{L}^2([c, d] \times [e, f])$, however, one could also prove that such subspace is *dense* in \mathbb{H} , thus arguing that the tensor product basis system is sufficient to model functions of \mathbb{H} . Therefore, we will assume that each $x \in \mathbb{H}$, admits the decomposition:

$$x(u, v) = \sum_{i \in \mathbb{N}} \sum_{j \in \mathbb{N}} c_{i,j} g_i(u) h_j(v), \quad c_{i,j} = \langle x, g_i \otimes h_j \rangle \quad (\text{C.7})$$

Thanks to the existence of a bijection⁶ between \mathbb{N} and \mathbb{N}^2 we can rearrange the terms of the basis system in order to obtain one depending on a single index instead of two, namely $\{\phi_k(u, v)\}_k$ instead of $\{g_i(u) \otimes h_j(v)\}_{i,j}$. We can thus rewrite (C.7) as:

$$x(u, v) = \sum_{k \in \mathbb{N}} c_k \phi_k(u, v) \quad (\text{C.8})$$

In practical applications, one typically truncates the number of basis functions on the two univariate domains to K_1 and K_2 respectively, obtaining a total number of basis equal to $K := K_1 + K_2$. Let us now introduce the vector $\boldsymbol{\phi}(u, v) \in \mathbb{R}^K$, $\boldsymbol{\phi}(u, v) = [\phi_1(u, v), \dots, \phi_K(u, v)]^T$ and the matrix $\mathbf{C} \in \mathbb{R}^{T \times K}$ with elements $C[t, k] = c_{tk}$ containing the coefficients of basis projection of the random functions Y_1, \dots, Y_T , in such a way that:

$$Y_t(u, v) = \sum_{k=1}^K c_{tk} \phi_k(u, v) + \delta_t(u, v) \quad t = \dots, T \quad (\text{C.9})$$

where $\delta_t(u, v)$ is a projection error, which is present due to the truncation of the basis system to the first K terms. In the remainder of this section, we

⁶The authors want to thank Edoardo Marchionni for a fruitful discussion on this topic.

will neglect the projection error and identify the observed functions with the ones reconstructed from the first M basis.

Following the work of [Ramsay and Silverman \(2005\)](#) and exploiting representation (C.8), we aim to rephrase the eigenproblem (C.2) in a matricial form. The estimated covariance function can be expressed in matrix terms:

$$\begin{aligned}\hat{\gamma}_0(u, v; w, z) &= \frac{1}{T} \sum_{t=1}^T Y_t(u, v) Y_t(w, z) = \\ &= \frac{1}{T} \sum_{t=1}^T \sum_{l,m=1}^K c_{il} \phi_l(u, v) c_{im} \phi_m(w, z) = \\ &= \frac{1}{T} \boldsymbol{\phi}(u, v)^T \mathbf{C}^T \mathbf{C} \boldsymbol{\phi}(w, z)\end{aligned}$$

Suppose now that an eigenfunction ξ admits the decomposition:

$$\xi(u, v) = \sum_{l=1}^K b_l \phi_l(u, v) + \kappa(u, v) = \quad (\text{C.10})$$

$$= \boldsymbol{\phi}(u, v)^T \mathbf{b} + \kappa(u, v) \quad (\text{C.11})$$

where $\mathbf{b} = [b_1, \dots, b_K]^T = [\langle \xi, \phi_1 \rangle, \dots, \langle \xi, \phi_K \rangle]^T$ contains coefficients of basis projection of ξ .

Neglecting once again the projection error κ , the goal becomes now to estimate the coefficients \mathbf{b} and the corresponding eigenvalue λ for each eigenfunction ξ_j , for $j = \dots, M$. Let's introduce finally $\mathbf{W} \in \mathbb{R}^{K \times K}$, defined as $\mathbf{W} := \int_c^d \int_e^f \boldsymbol{\phi}(u, v) \boldsymbol{\phi}(u, v)^T du dv$, notice that the tensor product basis is composed by two orthonormal basis systems, the resulting tensor product basis system is itself orthonormal and thus $\mathbf{W} = \mathbf{I}$, where \mathbf{I} denotes the diagonal matrix. The lhs of (C.2) can be rewritten as:

$$\hat{\Gamma}_0 \hat{\xi}(u, v) = \int_c^d \int_e^f \frac{1}{T} \boldsymbol{\phi}(u, v)^T \mathbf{C}^T \mathbf{C} \boldsymbol{\phi}(w, z) \boldsymbol{\phi}(w, z)^T \hat{\mathbf{b}} dw dz = \quad (\text{C.12})$$

$$= \frac{1}{T} \boldsymbol{\phi}(u, v)^T \mathbf{C}^T \mathbf{C} \left(\int_c^d \int_e^f \boldsymbol{\phi}(w, z) \boldsymbol{\phi}(w, z)^T dw dz \right) \hat{\mathbf{b}} = \quad (\text{C.13})$$

$$= \frac{1}{T} \boldsymbol{\phi}(u, v)^T \mathbf{C}^T \mathbf{C} \mathbf{W} \hat{\mathbf{b}} \quad (\text{C.14})$$

The eigenequation thus becomes:

$$\frac{1}{T}\phi(u, v)^T \mathbf{C}^T \mathbf{C} \mathbf{W} \hat{\mathbf{b}} = \lambda \phi(u, v)^T \hat{\mathbf{b}} \quad \forall u, v \quad (\text{C.15})$$

$$\frac{1}{T} \mathbf{C}^T \mathbf{C} \mathbf{W} \hat{\mathbf{b}} = \lambda \hat{\mathbf{b}} \quad (\text{C.16})$$

We can hence derive the eigenvectors $\hat{\mathbf{b}}_j$ of $\frac{1}{T} \mathbf{C}^T \mathbf{C} \mathbf{W}$ and the corresponding eigenvalues and finally reconstruct the eigenfunctions $\hat{\xi}_j$ thanks to (C.11).

Appendix C.3. Comparison of Estimation Methods

In this section, we aim to compare the two proposed approach for performing functional principal component analysis, namely the basis expansion and the discretization approach. Without loss of generality, we will settle the study in $\mathcal{L}^2([0, 1] \times [0, 1])$.

In general, given a finite basis system $\{\phi_k\}_{k=1, \dots, K}$, one can represent a functional time series $\{Y_t\}_{t=1}^T$ by means of representation (C.9), that we report here for ease of reference:

$$Y_t(u, v) = \sum_{k=1}^K c_{tk} \phi_k(u, v) + \delta_t(u, v) \quad t = 1, \dots, T \quad (\text{C.17})$$

Starting from this decomposition, we have derived in [Appendix C.2](#) an estimator of the functional principal components ξ_j , which, however, neglects the contribution of the error δ_t . For such reason, the choice of the basis system $\{\phi_k\}_{k=1}^K$ is crucial, and when a meaningful option is not available, the approximation residual δ_t will be large and this procedure will inevitably provide biased estimates of ξ_j . On the other hand, the FPCA approach based on data discretization provides good result as long as the sampling grid is sufficiently dense.

In order to prove such thesis, we simulate a time series of functions $\{Y_t\}_{t=1}^T \subset \text{span}\{\phi_1, \dots, \phi_K\}$, from a non-concurrent FAR(1) process with Gaussian errors. Data are simulated based on a basis expansion on $\{\phi_1, \dots, \phi_K\}$, which is constructed as the tensor product basis of two Fourier basis systems $\{g_i\}_{i=1, \dots, K_1}$, $\{h_i\}_{i=1, \dots, K_2}$ both defined on $[0, 1]$. The sample size is chosen equal to $T = 50$, the number of basis in each of the one-dimensional systems is selected equal to 5, in order to have a total number of basis $K = 25$.

FPCA method	EFPC's		
	1st FPC	2nd FPC	3rd FPC
Basis on B-Spline	$2.62 \cdot 10^{-3}$	$4.45 \cdot 10^{-3}$	$2.28 \cdot 10^{-3}$
Discretization	$7.69 \cdot 10^{-4}$	$2.45 \cdot 10^{-3}$	$1.38 \cdot 10^{-3}$

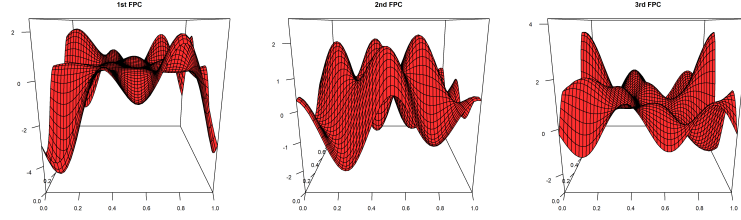
Table C.1: MSE between estimated FPC's on the basis system used for the simulation and FPC's estimated using another basis system or the discretization approach.

Since we know the space where the functions are embedded, we can apply the estimation procedure in [Appendix C.2](#) using as basis system the same one used in the simulation. Notice that in this case the approximation error δ_t in (C.17) will be exactly zero and one can derive optimal estimates of the functional principal components. Estimators of the first three functional principal components are represented in [Figure C.17a](#). We repeat the same estimation procedure, this time modelling functions with a basis built from the tensor product of two one-dimensional cubic B-Spline basis systems with 5 basis each. In this case, the basis system do not coincide with the one from which functions are simulated. Nevertheless, as reported in [Figure C.17b](#) all the scaled eigenfunctions are very close to the optimal ones estimated before. Finally, we compare the aforementioned estimators with the ones coming from the discretization approach. Each of the one-dimensional grids is discretized using a step size equal to 0.02, thus resulting in a total of 2500 points. Also in this case (see [Figure C.17c](#)), estimated harmonics are very close to the optimal ones in [Figure C.17a](#).

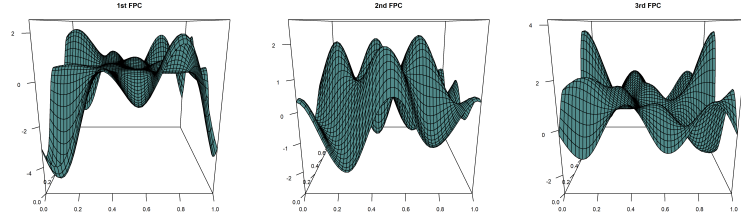
To enable for better comparison, we report in [Table C.1](#) the Mean Squared Error (MSE) (C.18) between the FPC's y estimated using full knowledge of the basis system from which functions are simulated and the ones estimated using other techniques (\hat{y}). Such quantity is computed starting from values of y and \hat{y} on a two-dimensional grid $\{(u_i, v_j)\}_{i=1, \dots, N_1; j=1, \dots, N_2}$.

$$MSE(y, \hat{y}) = \frac{1}{N_1 N_2} \sum_{i=1}^{N_1} \sum_{j=1}^{N_2} (y(u_i, v_j) - \hat{y}(u_i, v_j))^2 \quad (\text{C.18})$$

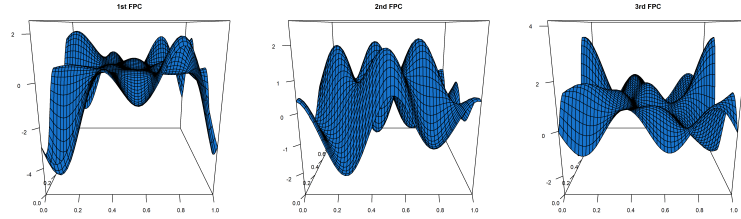
We can appreciate very low values of MSE, regardless of the technique used for FPCA, thus suggesting that both the basis expansion and the discretization approach are valid options on a practical point of view.



(a) FPCA by basis expansion on the same basis system used for the simulation.



(b) FPCA by basis expansion on a different basis system.



(c) FPCA by grid discretization.

Figure C.17: First three functional principal components, estimated with three different methods. As usual in PCA, EFPC's are unique up to a constant. For such reason, in order to compare the different approaches, estimated harmonics in the second and third row are each rescaled by means of the mean difference ratio with the ones in the first row.